Malter effect mechanism study in PNPI and MEPhI (Sarov)

G. Gavrilov, M. Buzoveria

28.11.2017

Study of Malter effect appearance mechanism

To remind: **$CF_3^\bullet$, $F^\bullet$, $O^\bullet$** are produced in avalanche at dissociation energy 3 ÷ 6 eV

$$e^- + CF_4 \rightarrow CF_3^\bullet + F^\bullet + e^-; \quad (1)$$

$$e^- + CF_4 \rightarrow CF_3^\bullet + F^-; \quad (2)$$

$$e^- + CF_4 \rightarrow CF_2^\bullet + 2F^\bullet + e^-; \quad (3)$$

$$e^- + CO_2 \rightarrow CO^\bullet + O^\bullet + e^-; \quad (4)$$

$$e^- + CO_2 \rightarrow CO^\bullet + O^-; \quad (5)$$

$$e^- + CO_2 \rightarrow CO^- + O^\bullet. \quad (6)$$

❖ Presence of **$O^\bullet$** stimulates additional generation of **$F^\bullet$** which provides etching of Si and other organics

$$O^\bullet + CF_3^\bullet \rightarrow COF_2^\bullet + F^\bullet; \quad (7)$$

$$O^\bullet + CF_2^\bullet \rightarrow COF^\bullet + F^\bullet; \quad (8)$$

$$e^- + COF_2 \rightarrow COF^\bullet + F^\bullet + e^-; \quad (9)$$

$$O^\bullet + COF^\bullet \rightarrow CO_2\uparrow + F^\bullet. \quad (10)$$

Si deposits cleaning by **$F^\bullet$**

$$4F^\bullet + Si \rightarrow SiF_4\uparrow;$$

$$4F^\bullet + SiO_2 \rightarrow SiF_4\uparrow + O_2\uparrow;$$

$$Si + CF_3^\bullet + F^\bullet + 2O \rightarrow SiF_4\uparrow + CO_2\uparrow.$$

This “thin film” or “finger traces” model is well tested at recover of the LHCb muon chambers

- ❑ To provide an effective cleaning from silicon and organic deposits a high current about of 20-40 μA is needed, that takes
- ❑ Etching rate can be accelerated with adding O2 in the gas mixture.

Study of Malter effect appearance mechanism

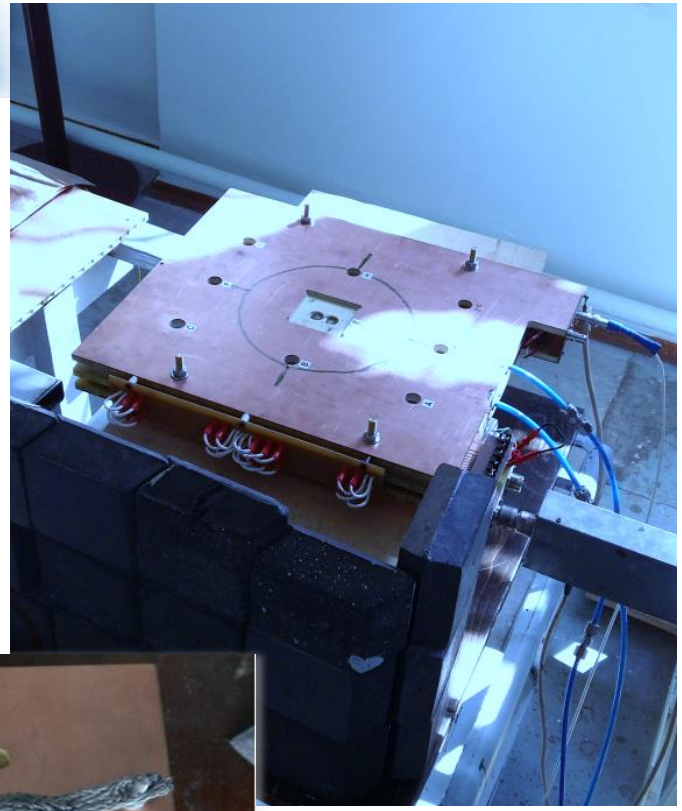

New aging tests are necessary:

- due to hard radiation conditions at future HL-LHC
- due to first manifestations of Malter effect in CSC
- to find eco-friendly solution for CF4 outlet reducing

Small scale CSC prototype module for aging study

- 2 planes, each with 7 controlled anode wires;
- 50 μm gold-coated anode wire;
- 285 x 340 mm^2 sensitive area, 1670 cm^3 gas volume;
- S = 3 mm ;
- L = 4.5 mm ;
- Identical geometry and construction materials to CSC ;
- Strip resistance control at specially ; cut strips on the cathode plane ;
- Gas flow during aging test was 4 sccm ; that is ~ 3.5 Volume per day ;
- No gas recirculation was applied.

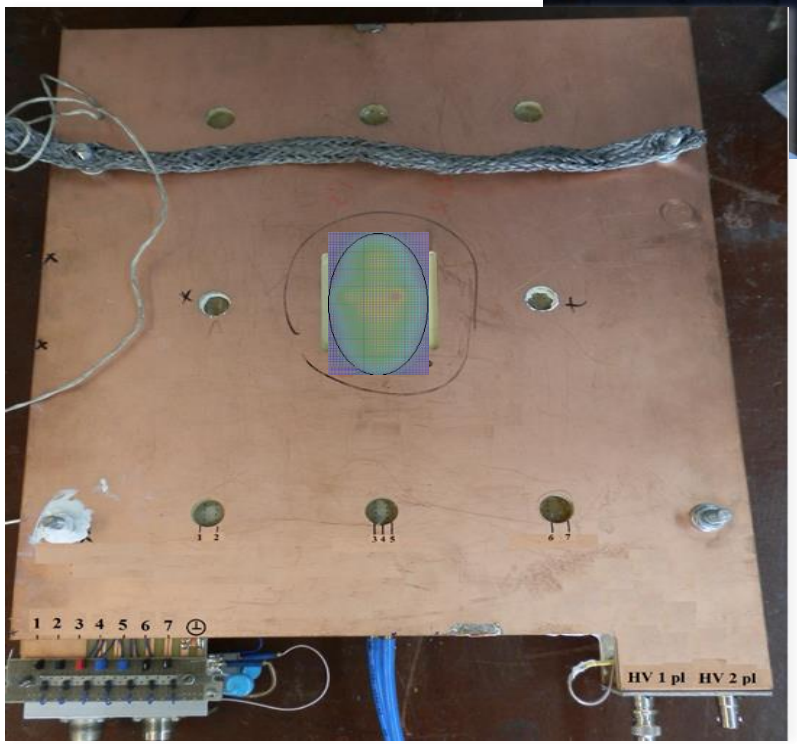

BUT

* Readout from anode wires only ;

* - HV applied to the cathode.

Targeting aging tests in PNPI

- First local aging test under ^{90}Sr irradiation was performed with compact CSC prototype module fed by standard CSC gas mixture;
- 1.36 C/cm accumulated charge is obtained, that is 7× of the expected charge after 3000 fb^{-1} at HL-LHC. The absence of amplitudes degradation matches with the previous tests in 1999 -2001;
- Strip-to-strip resistance dropped during the aging test from 5×10^{13} Ω up to 5×10^{7} Ω;
- Despite of the strong oxidation and Si coating on cathodes surface, no Malter current manifestation have been found;
- Test results can be a benchmark for the future study of the eco-friendly gas mixtures;

Study of Malter effect appearance mechanism

Irradiation zone on the anode plane
$\pi \times 3.7/2 \times 2.0/2 \approx 5.8$ cm^2

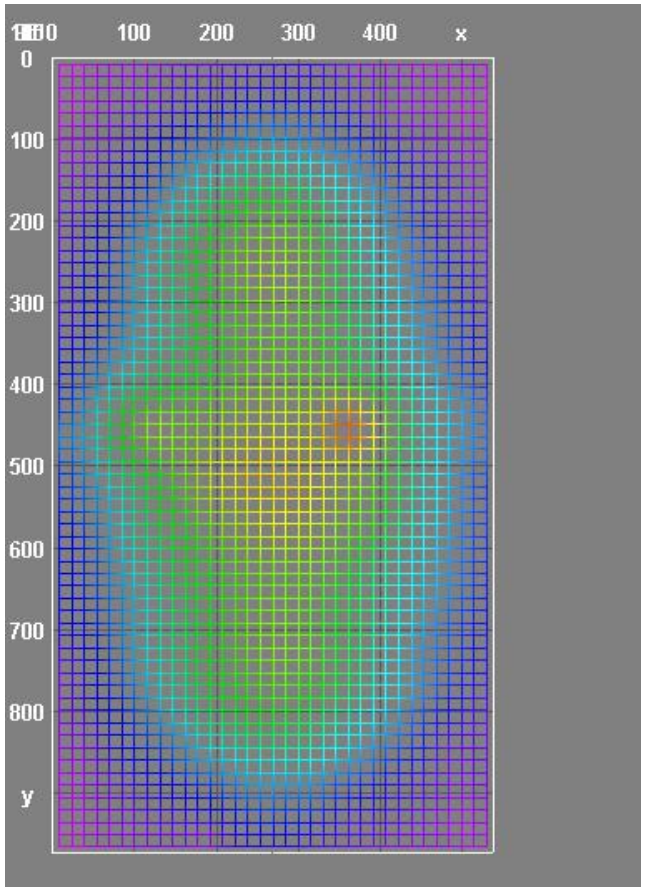

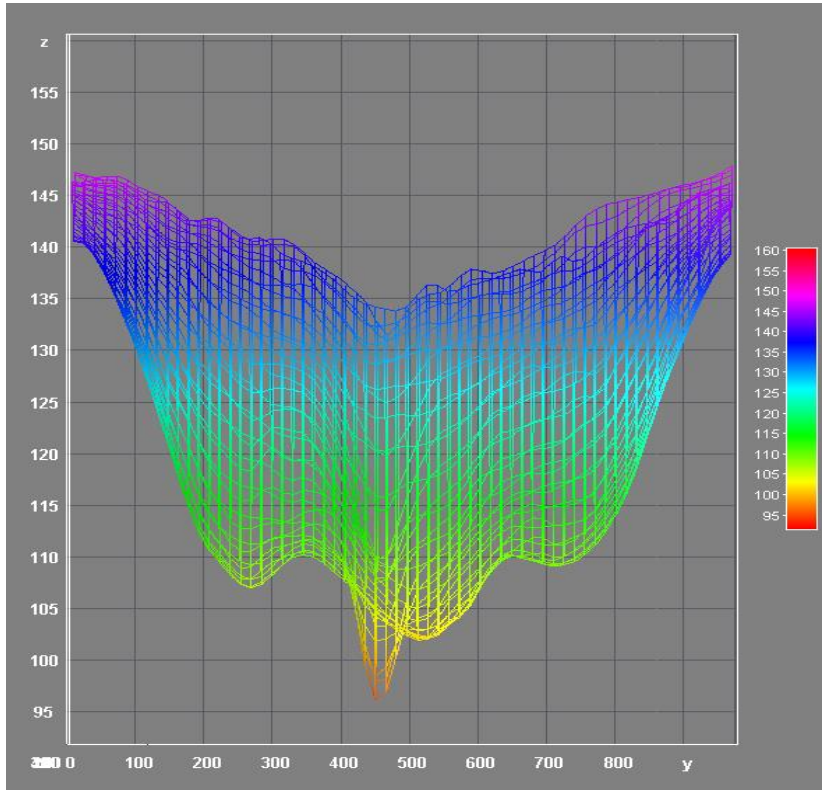

Along anode wires

- Work point set HV=3750 V GG=5×10^4
  Ionization current at work point is 17 μA per 6 cm^2 or
  1 μA per 1 cm of wire length
  1.45×10^6 Hz per 1 cm of wire length

- This kind of aging test is actual for longevity evaluation of the CSC modules in extremal conditions and upper estimate of the anode wires aging.

- Irradiation zone is a generator of the radicals and ions, which diffuse around in the gas volume of the CSC prototype.

- The CSC-CMS comparable damages of the cathode surface in the aged CSC prototype can be found only in the intermediate zone in the not irradiated area.

SEM image of the copper foil surface of not irradiated FR4

Roughness profile has a depth of 0.4 μm

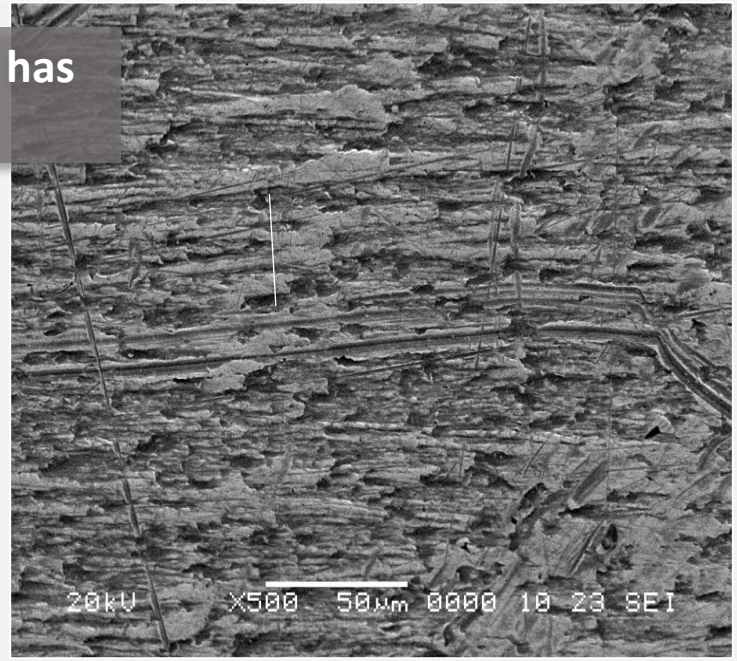

Force microscopy of original FR4

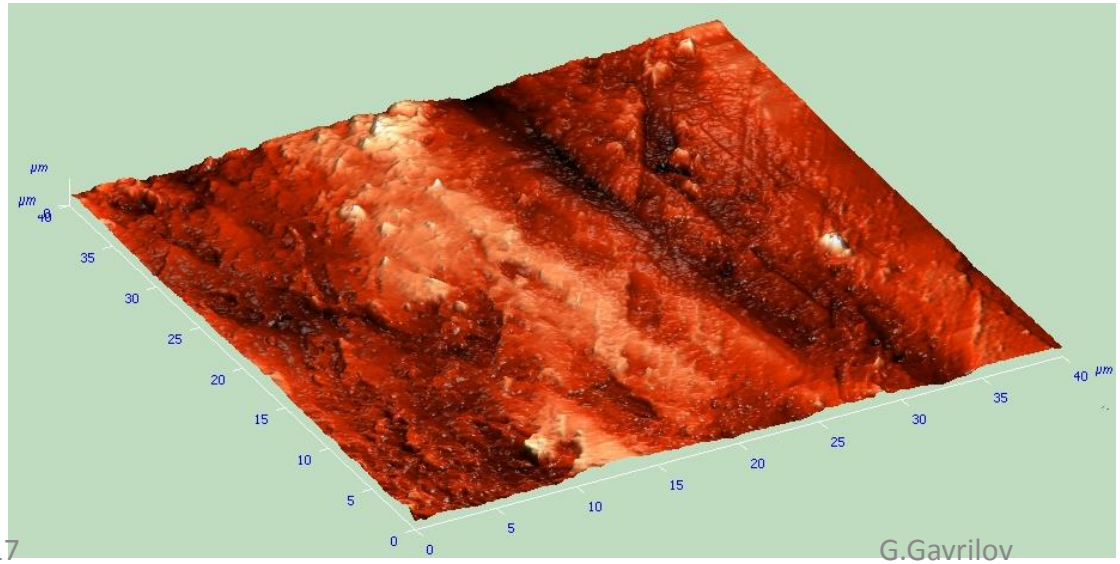

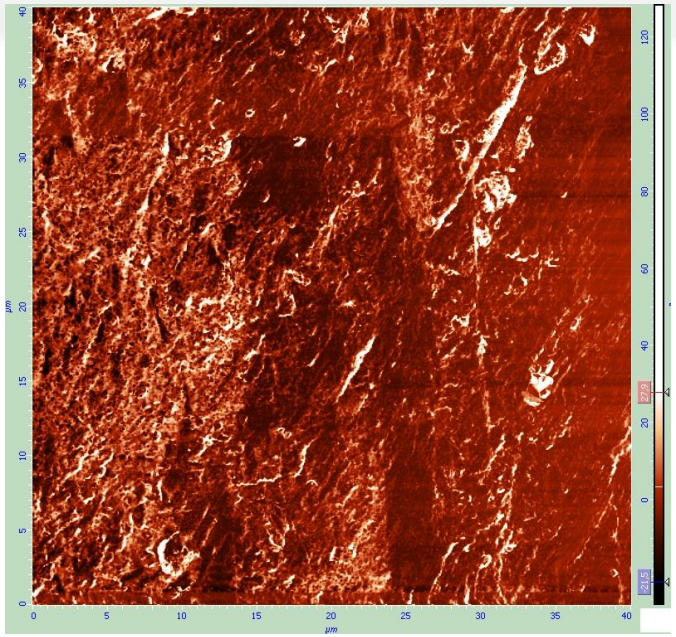

Study of Malter effect appearance mechanism

Field structure in vicinity of the cathode plane:

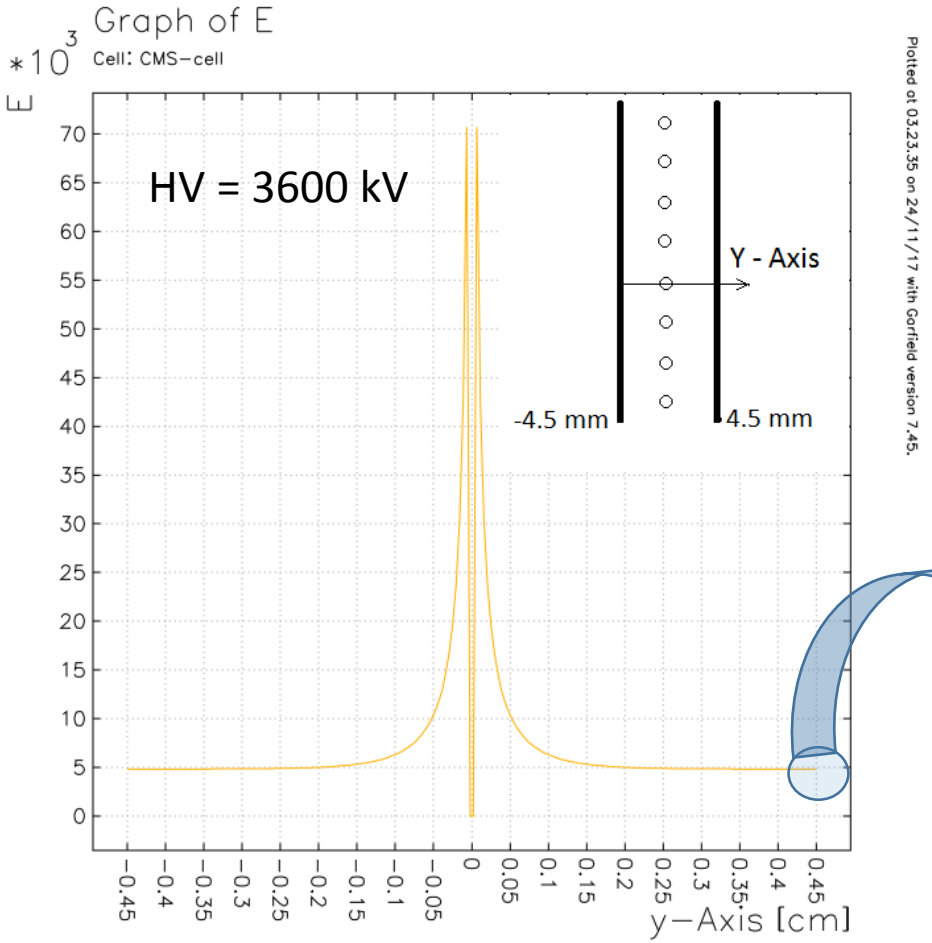

…60 µm apart from the cathode plane

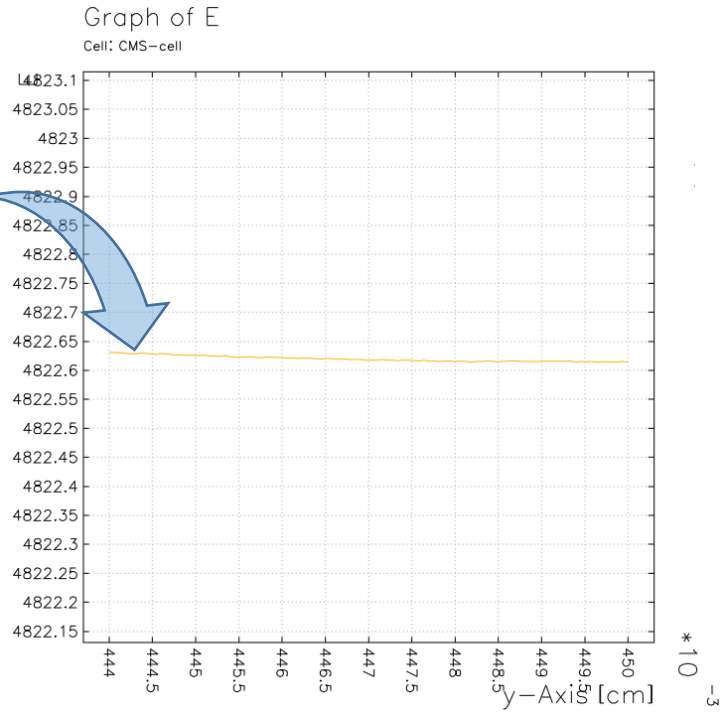

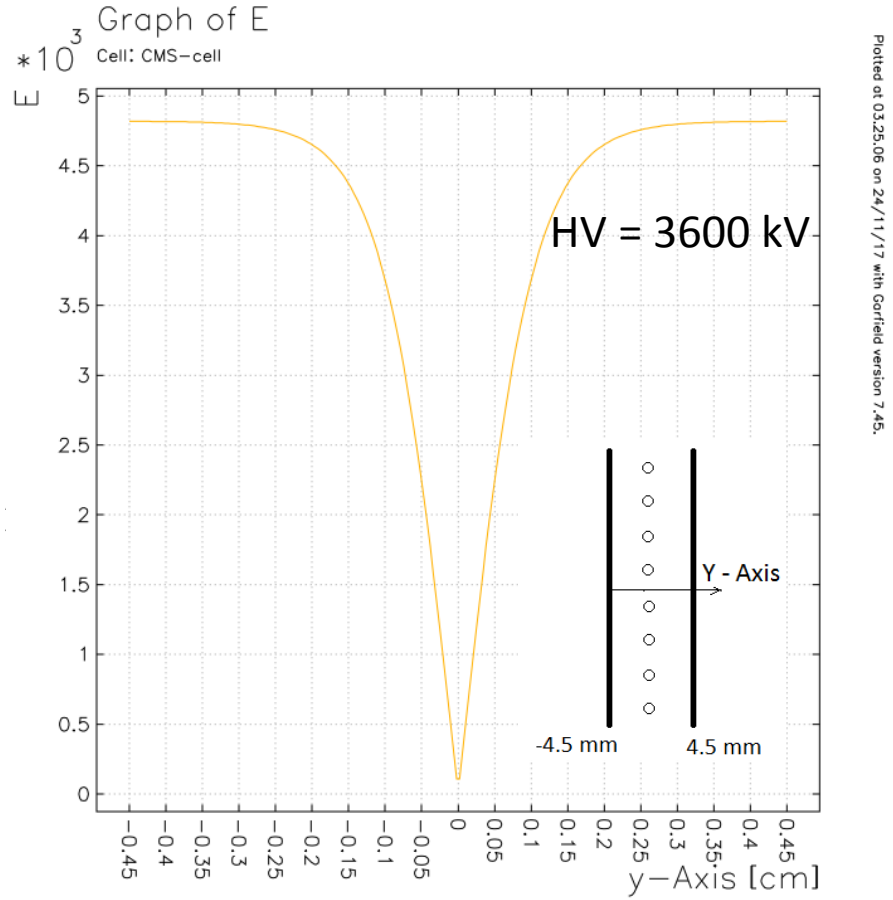

The electric field strength on the CSC cathode planes is ~ 5000 V/cm

Photos of the disassembled detector after accumulation of Q=1.36 C/cm with 40%Ar+50%CO_2+10%CF_4

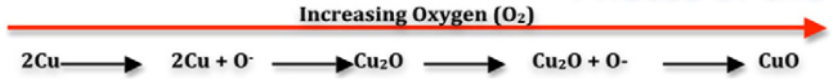

$10^3 – 10^8$ Ωm ·cm 0.01 – 1 Ωm · cm

Simplified illustration of the oxidation reaction of copper for the formation of Cu_2O and CuO.

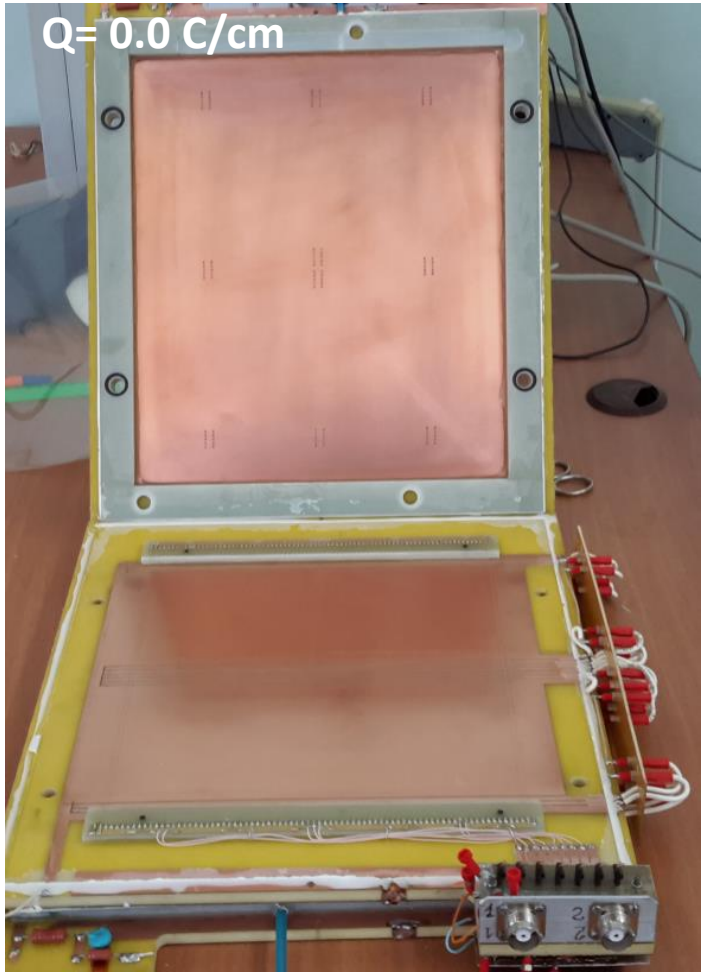

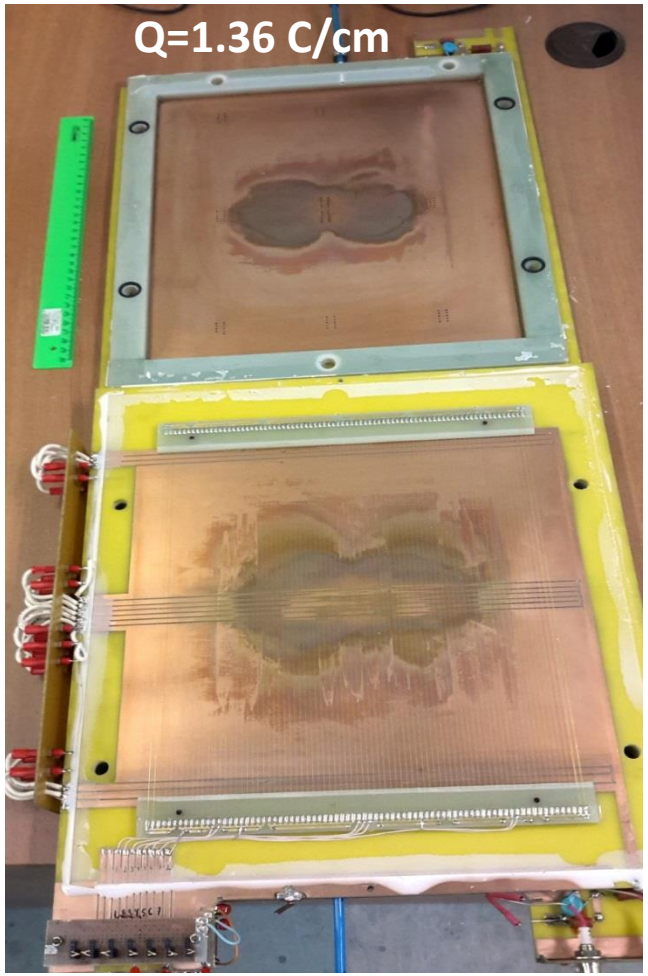

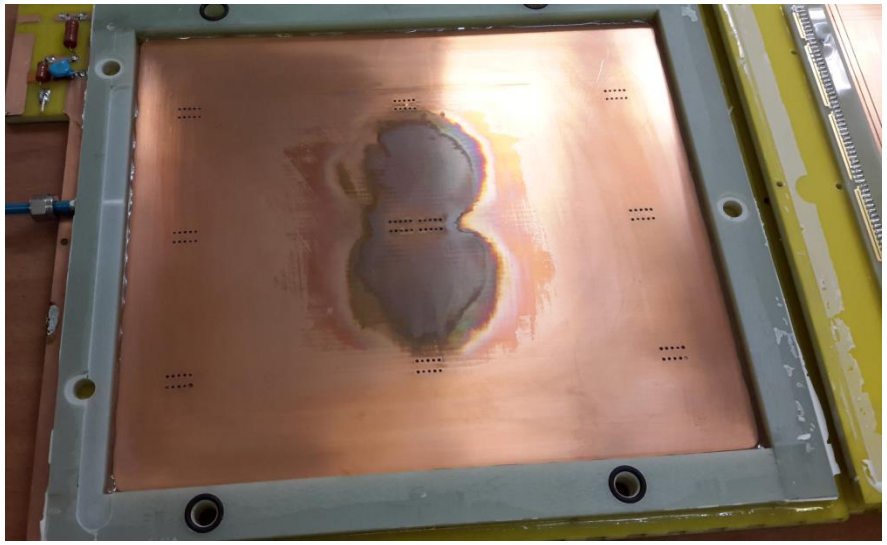

Upper cathode plane

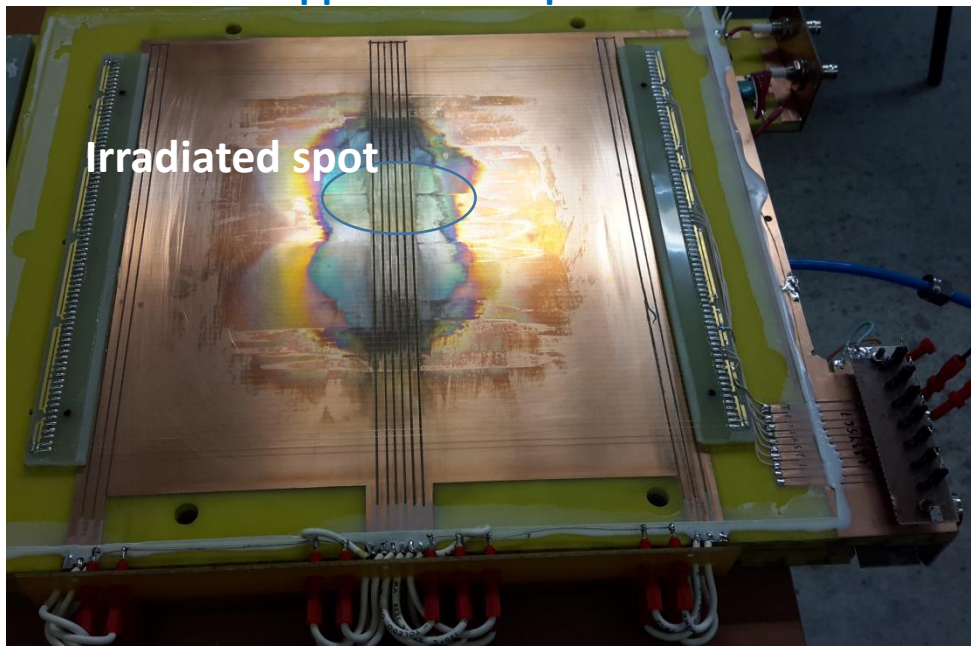

Bottom cathode plane

Damaged (toughed by oxidation) zone is >>10 times bigger of irradiated spot (~6 cm2) ➡ Main source of cathode aging are the radicals from O_2

Aging results from GIF (1999)

$$2Cu + 1/2O_2 \rightarrow Cu_2O.$$

$$Cu_2O + 1/2O_2 \rightarrow 2CuO.$$

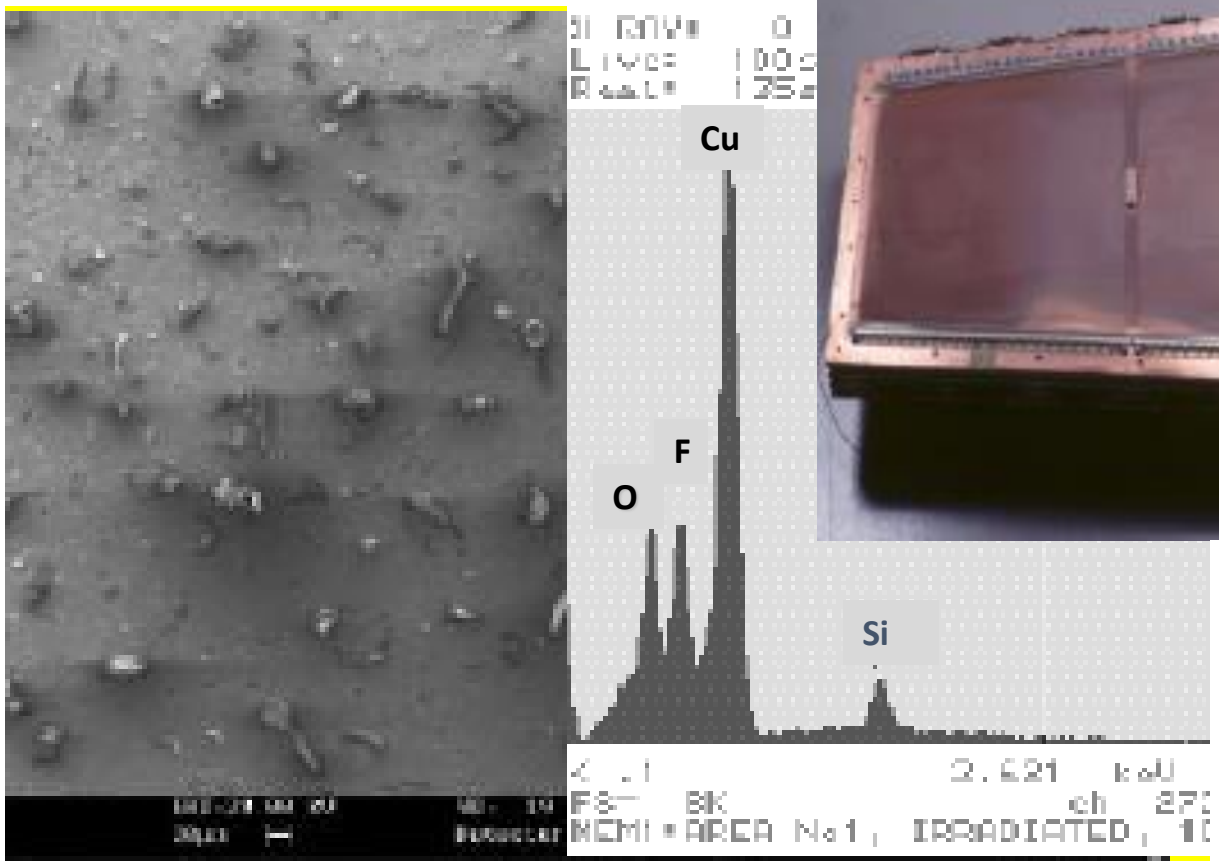

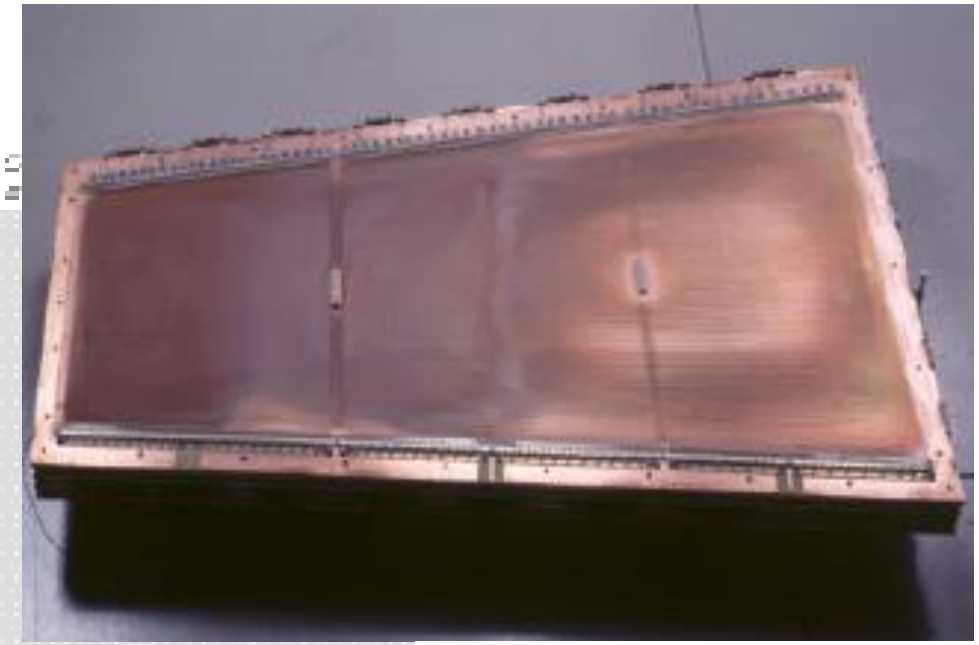

Only left half of the CSC module was irradiated.

Accumulated charge 0.3 C/cm
Oxidation touched both parts of the module

D. Acosta et al. NIMA 515 (2003) 226–233

Targeting aging tests in PNPI

- Second aging test under ^{90}Sr irradiation was performed with compact CSC prototype module fed by 36.6%Ar+61.75%CO_2+1.65%CF_4 gas mixture
- 0.39 C/cm accumulated charge is obtained
- Strip-to-strip resistance dropped during the aging test from 2×10^{13} Ω up to 1×10^{11} Ω
- At accumulated charge ~0.3 C/cm exceeding HL-LHC an appearance of Malter currents was observed
- Dedicated studies of the cathode surface are ongoing

Photos of the disassembled detector after accumulation of Q= 0.39 C/cm aged with $36.6\%Ar+61.75\%CO_2+1.65\%CF_4$

Damaged zone is just few times bigger of irradiated spot 8 cm^2

Malter current ~100 μA was obtained at the end of the tests !

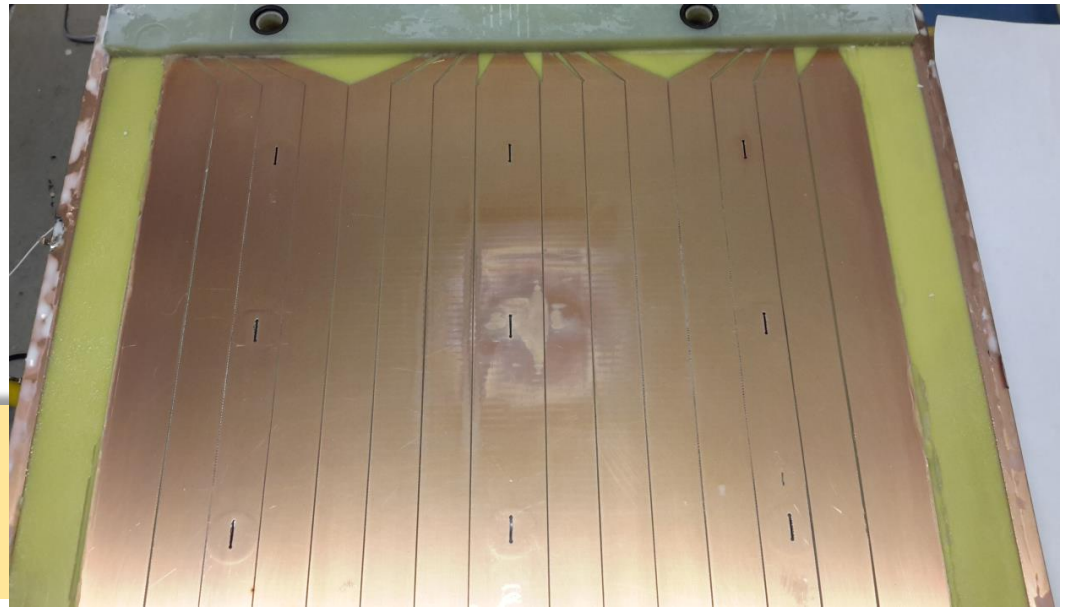

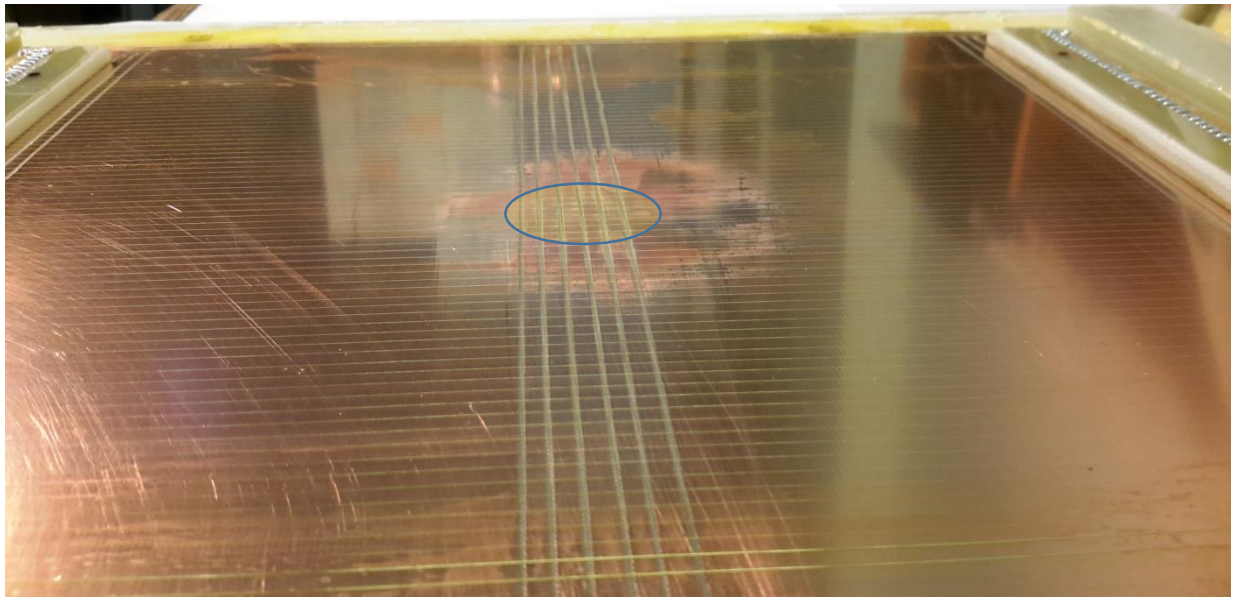

G.Gavrilov

Study of Malter effect appearance mechanism

Due to irradiation, the copper foil on the cathode oxidizes and becomes uneven and rough covering the area bigger of the irradiated zone:

- For the test with 10%CF_4 ($Q_{total} \approx 27$ C) the damaged (or oxidized) area is 580 cm^2 that is ~100 times bigger of the irradiated zone
- For the test with 1.6%CF_4 ($Q_{total} \approx 10$ C) the damaged (or oxidized) area is 56 cm^2 ~ 7 times bigger of the irradiated zone

To extrapolate the cathode foil damage after CSC prototype aging tests on "uniformly" irradiated CSC modules the samples from not irradiated zone have to be considered

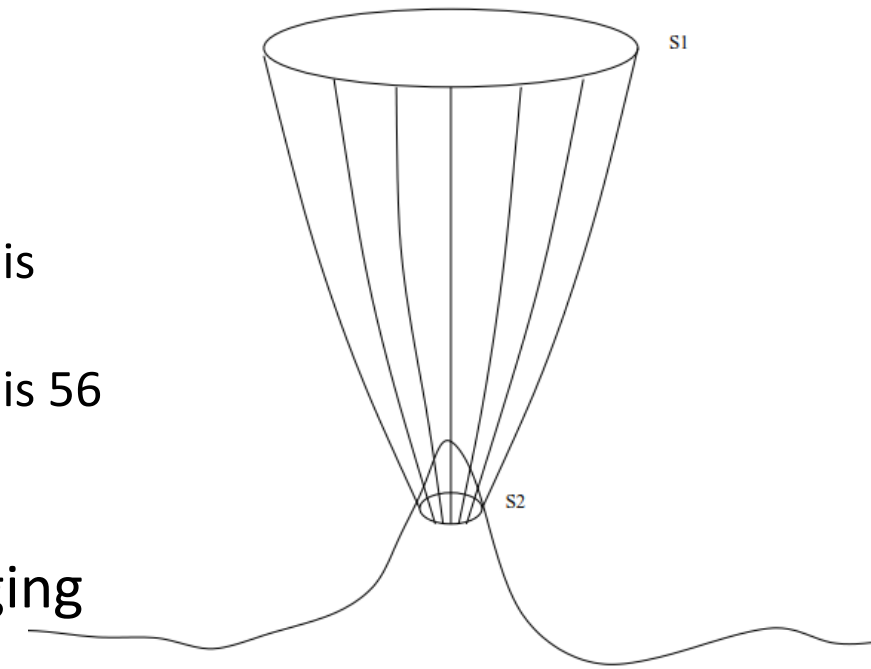

Positive ions current and polarised polymers flow is S2/S1 times bigger on the peaks

Ions current density through the peak is
$j = j_i \times S/\pi r^2$,
S- peak surface area, r – peak radii, j_i - ions flux density.

For cylinder peak $j = j_i \times 2h/r$ (h – height)
For conical $j = j_i \times \ell/r$ (ℓ - length of slope)

Study of Malter effect appearance mechanism

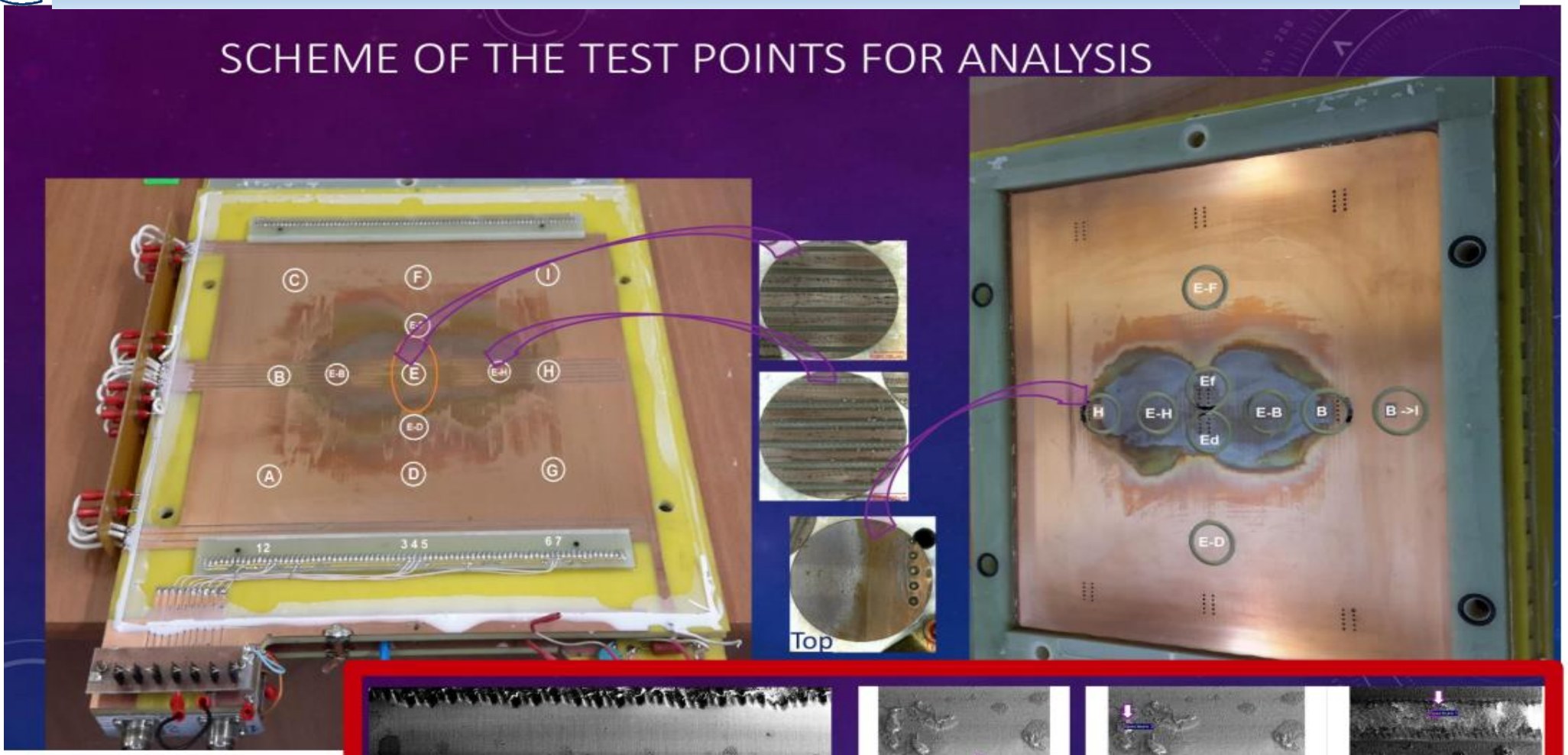

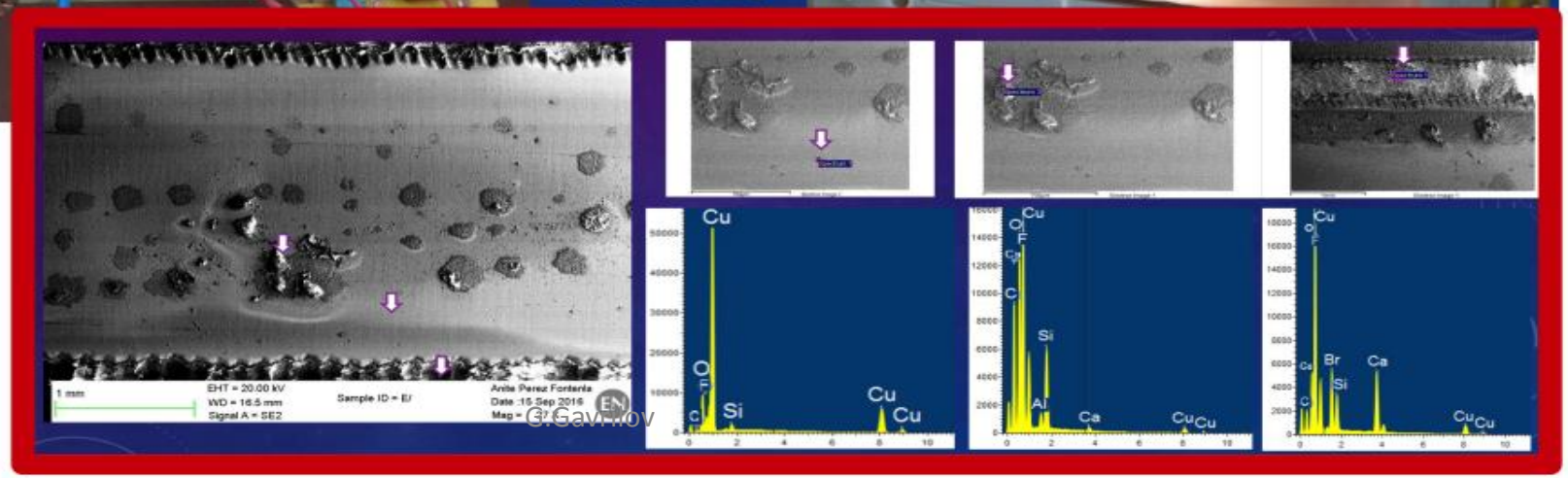

Sample "E":

Cu, O, Si, F

CSC CMS prototype longevity test in PNPI

- Small (<0.1cm^2) samples from E and B-I (most irradiated and “reference”)
- Zeiss XB540 FIB/SEM with Oxford Instruments X-Max Silicon Drift Detector
- Use of FIB=”Focused Ion Beam” for milling a x-section

FIB cross section – 5 µm depth milling of sample E

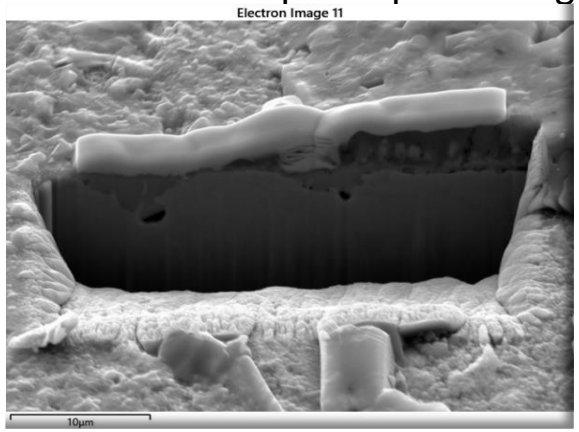

FIB – Focused Ion Beam

EDS mapping and SEM image of sample E small FIB cross section – zoomed 1.

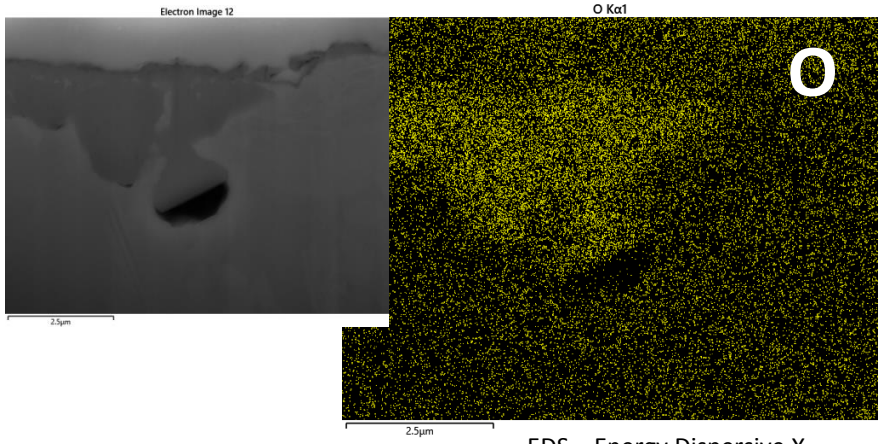

EDS – Energy Dispersive X-ray spectroscopy

Sample E - surface

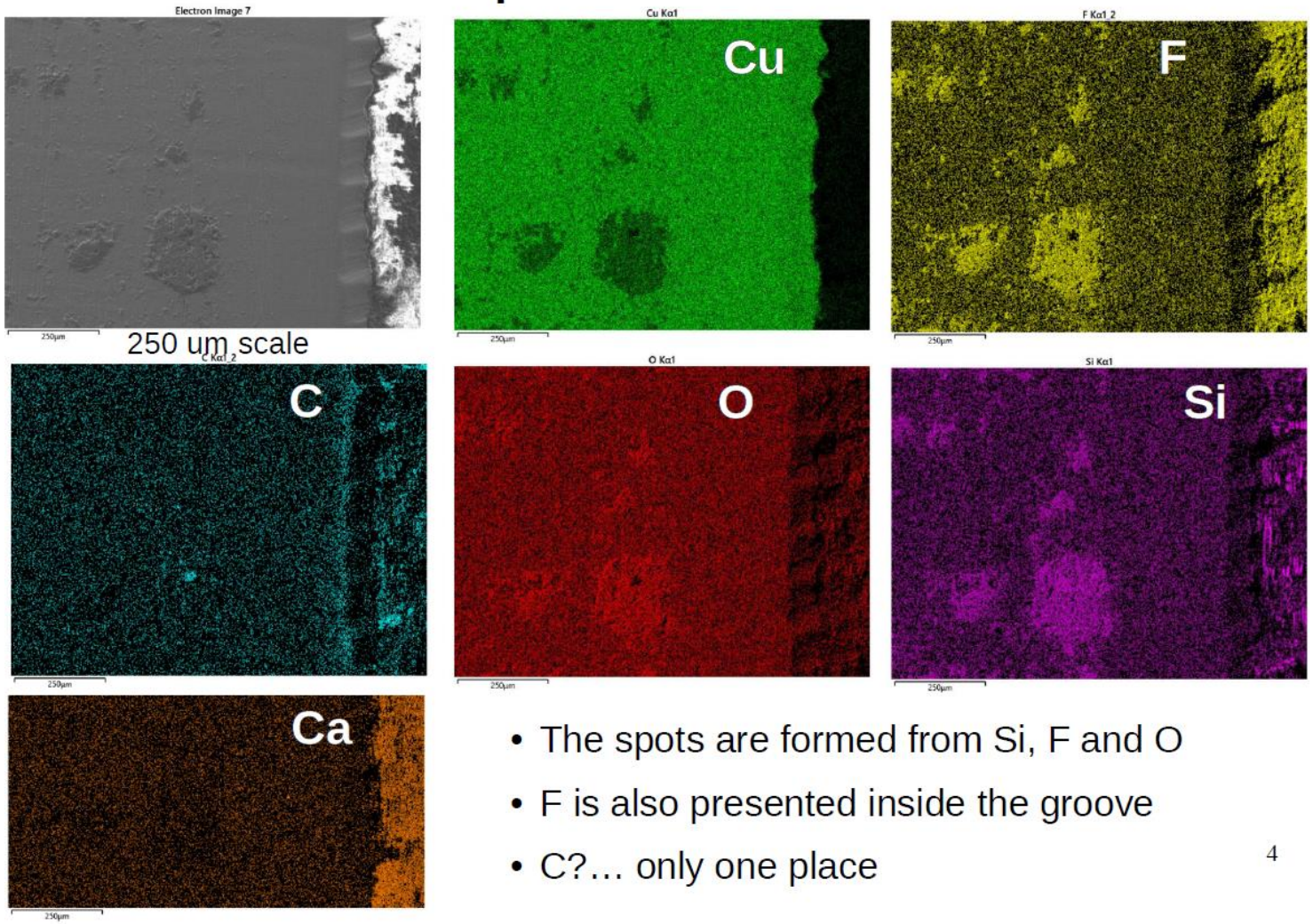

- The spots are formed from Si, F and O
- F is also presented inside the groove
- C?… only one place

CSC CMS prototype longevity test in PNPI

Sample B-I - surface

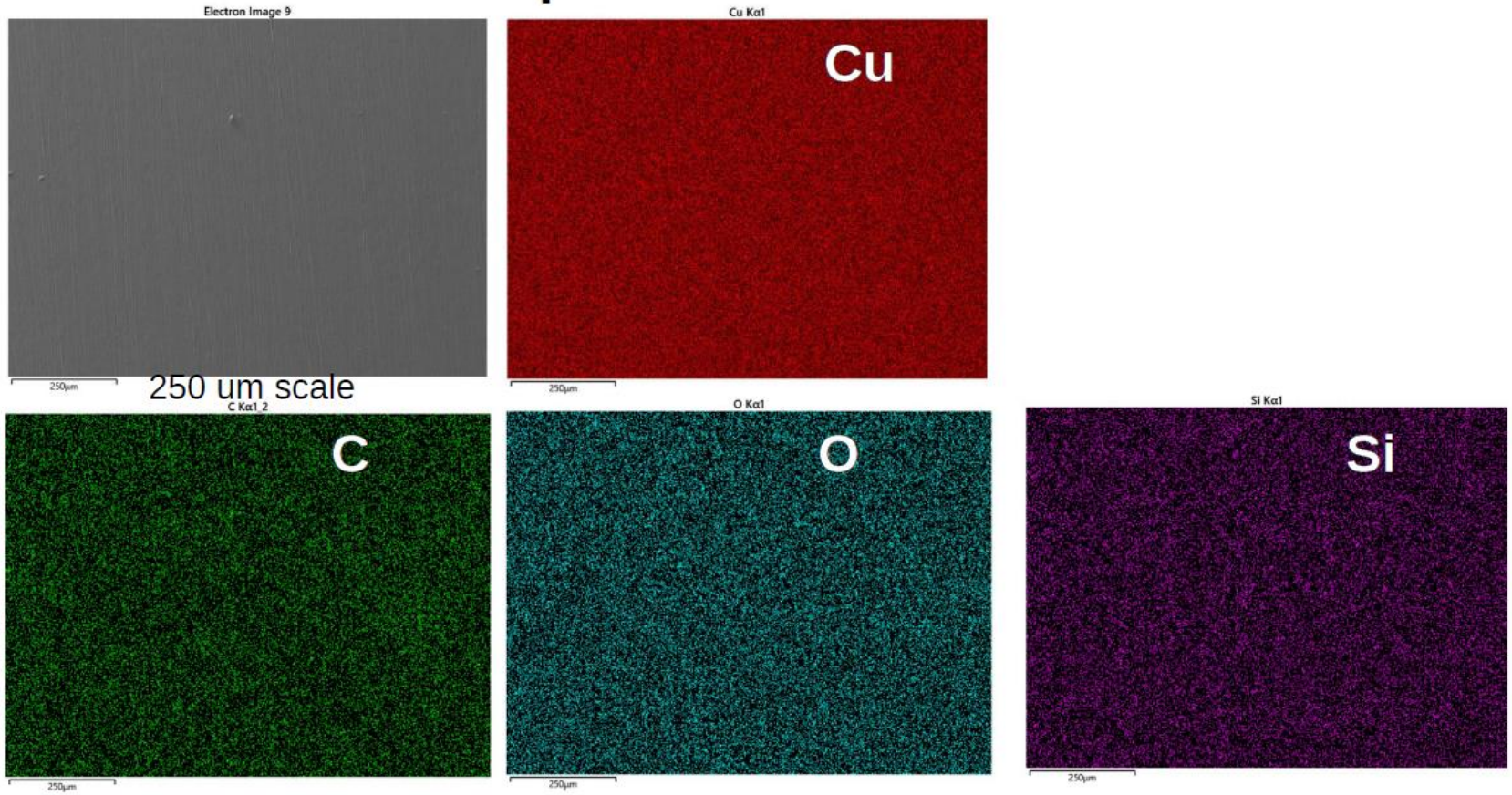

Weight fractions averaged over analysis surface (indicative ONLY!)

Element	Cu (wt%)	O (wt%)	C (wt%)	F (wt%)	Si (wt%)	Ca (wt%)
Sample B-I	84.5 ± 0.1	3.0 ± 0.0	12.3 ± 0.1	0.0	0.3 ±0.0	0.0
Sample E	73.4 ± 0.1	11.5 ± 0.0	8.0 ± 0.1	4.6 ± 0.1	1.8 ± 0.0	0.7 ± 0.0

5

Sensitivity depth – O(um), different for different elements!

Study of Malter effect appearance mechanism

The physicists from National Research Nuclear University MEPhI (Sarov) took participation in the study of the samples from the aged CSC Prototype, too …

Cathode FR4 samples from the points E-D, E-D, H, E^f were analysed with

- Atomic Force Microscope microscopy with “Solver Next”;
- Nuclear scanning microprobe analysis.

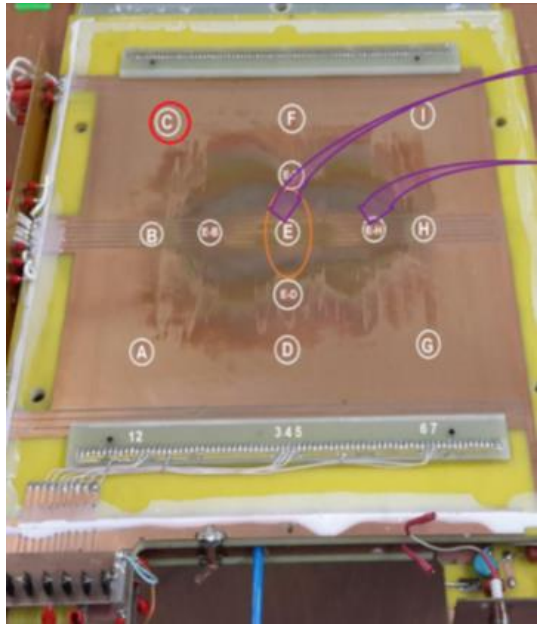

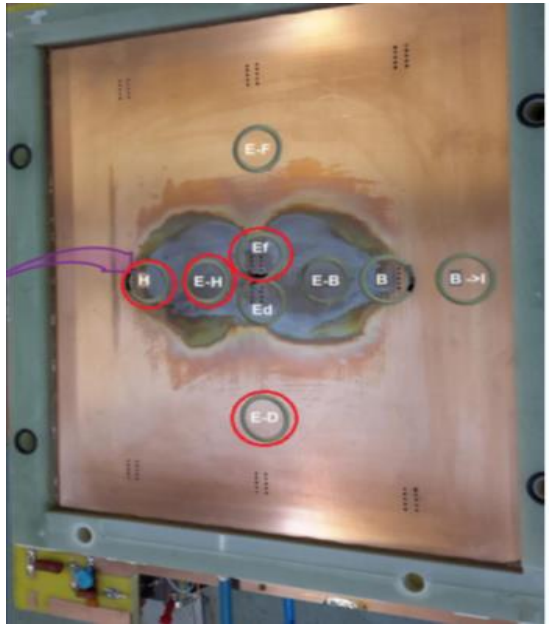

- # Nuclear scanning microprobe setup (EGP-10)

  - E=14 MeV H^+ beam with not less of ±300 µm spot on the target
  – Scanning rate from point-to-point 200 µs.
  – Time of positioning less of 40 µs.

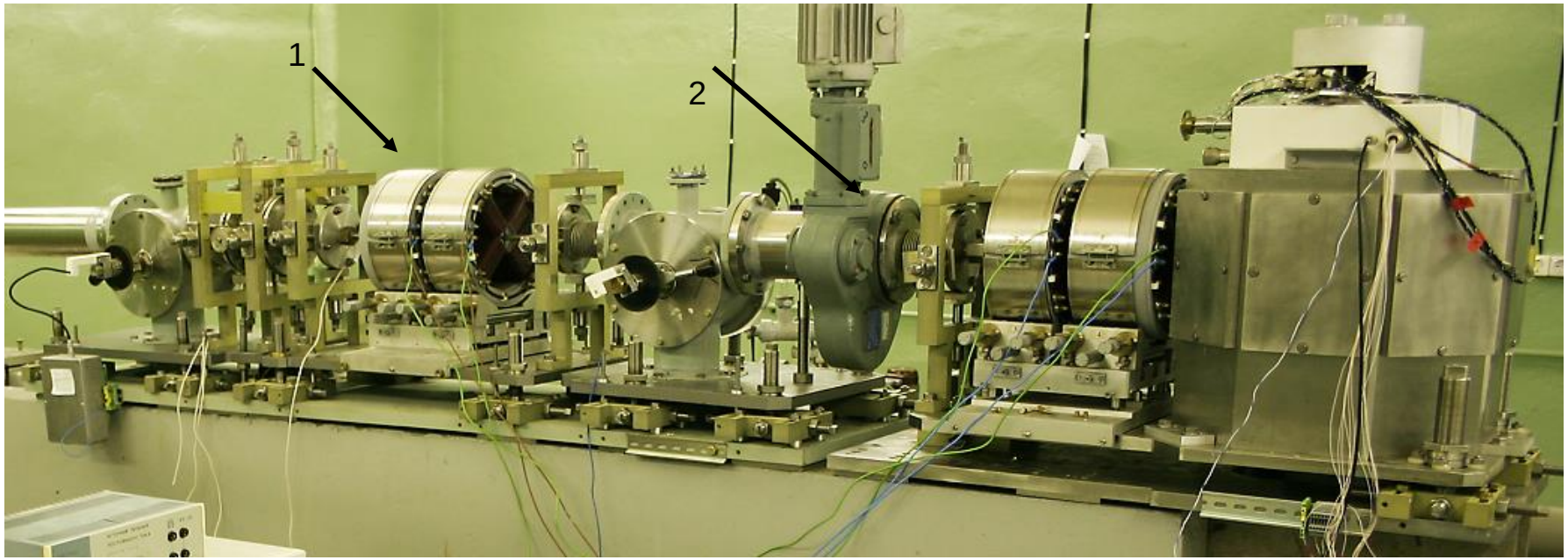

1 – Ions optical focusing system; 2 – beam-sample interaction chamber

Reference point C

Force microscopy analysis of the surface structure

Evaluation of surface roughness

Detection of micro damages on the surface - blisters

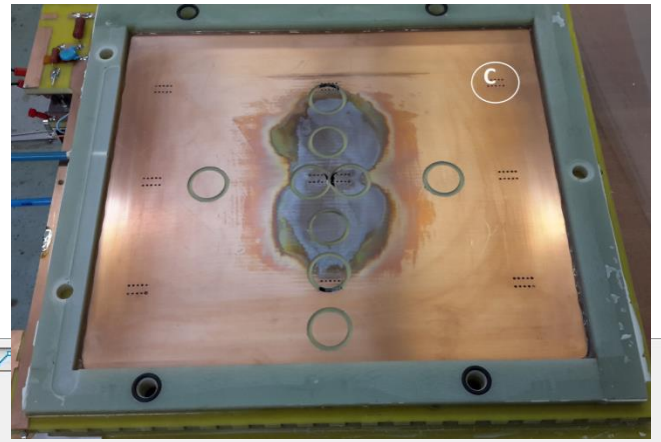

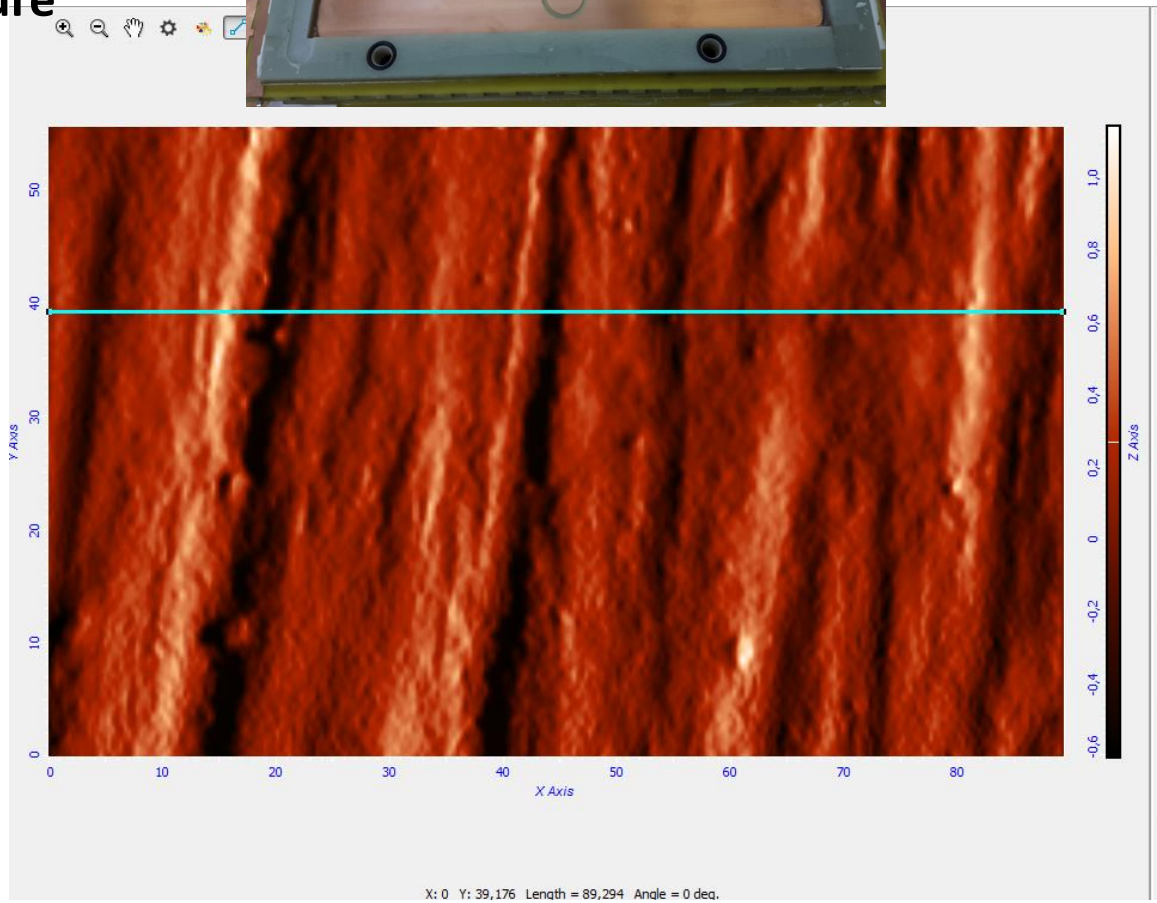

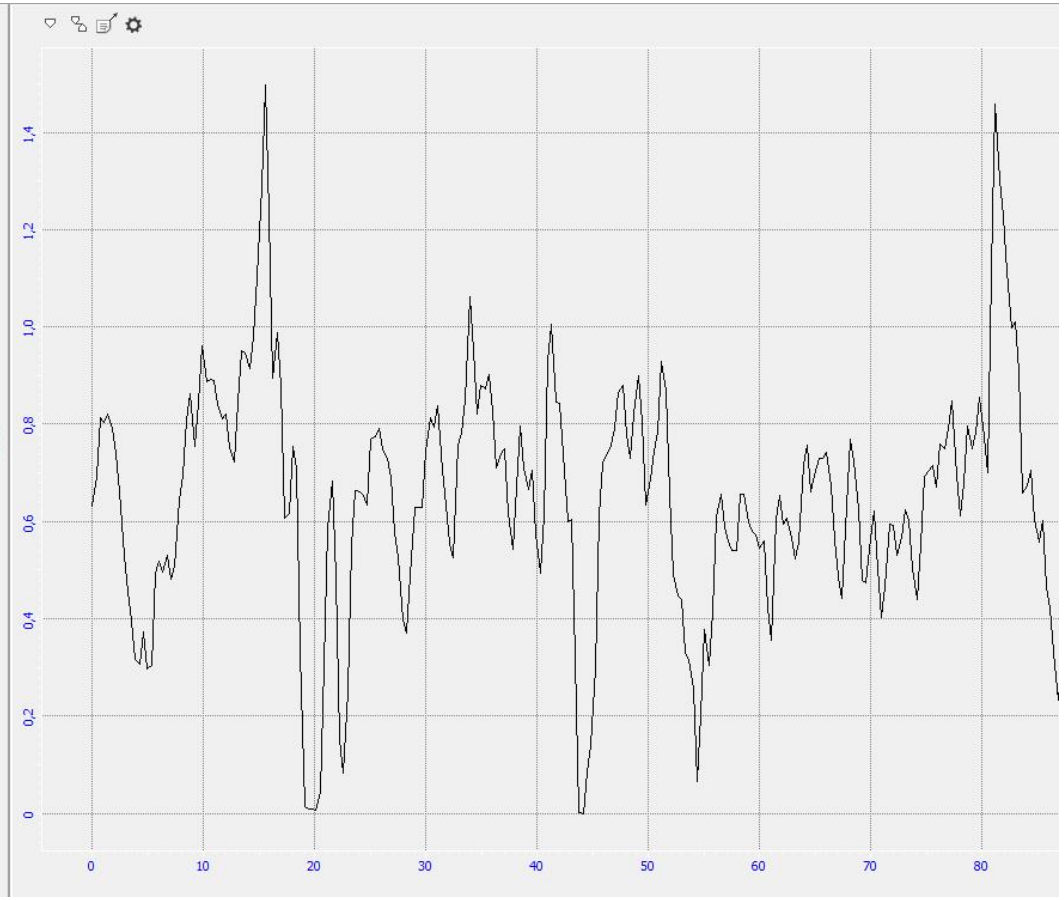

Sample E-D from intermediate zone

The blisters are often formed on the traces of machining, along the boundaries of structural formations. This photo is typical for the described case. Vesicles (blisters) are formed along the fibres

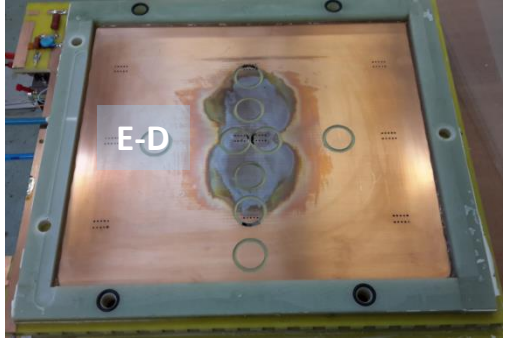

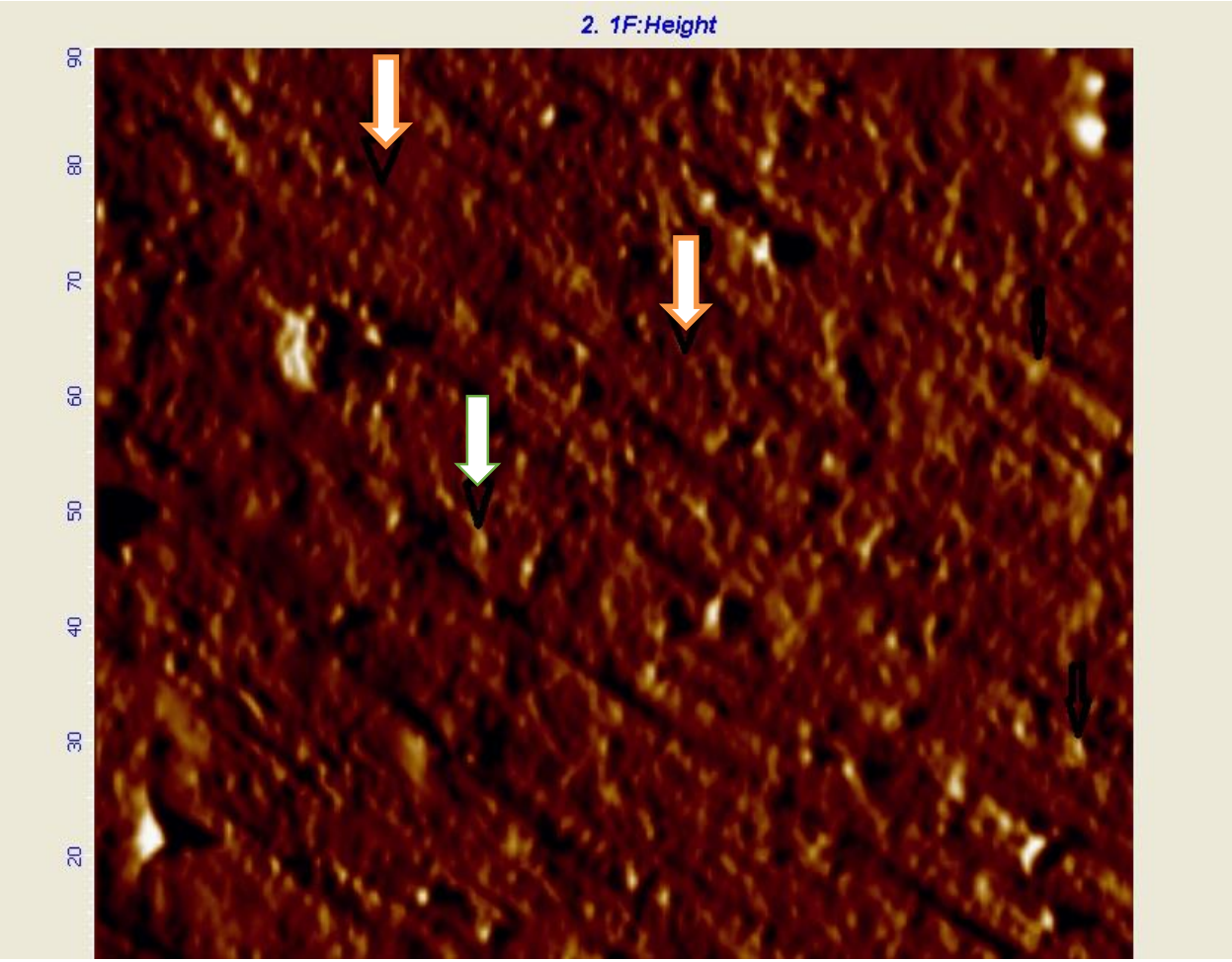

90 ×90 μm

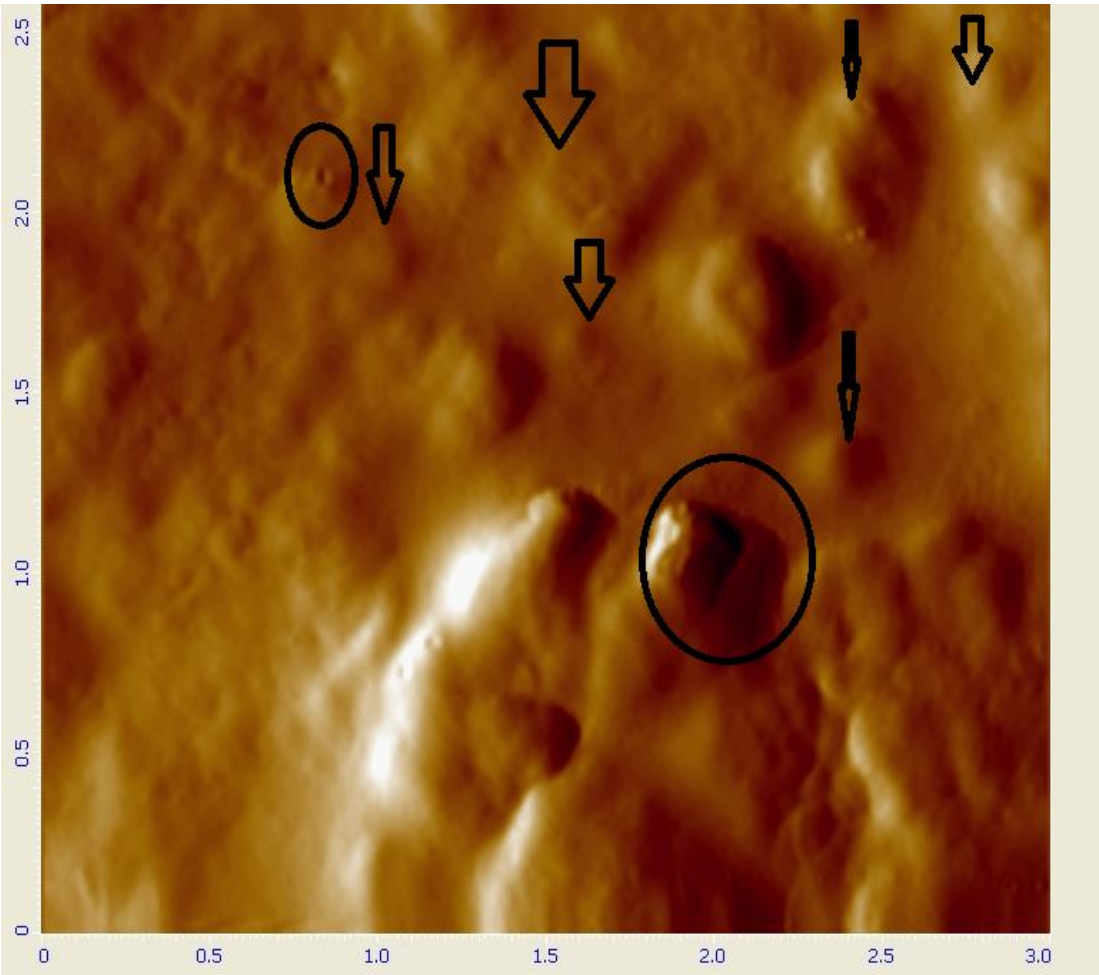

3 × 3 μm

Sample E-D

Roughness varies greatly even within the same sample and increase toward the irradiation zone

90 × 90 μm areas	Surface profile along ~120 μm line	Roughness
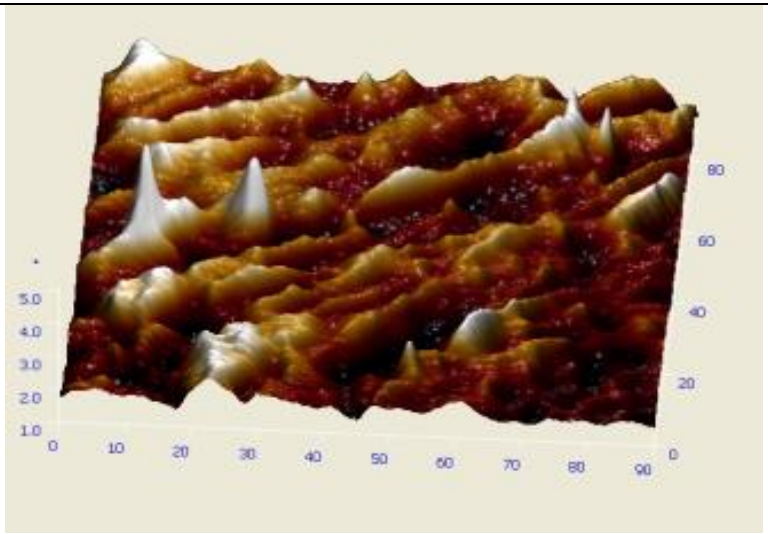	0.12 μm 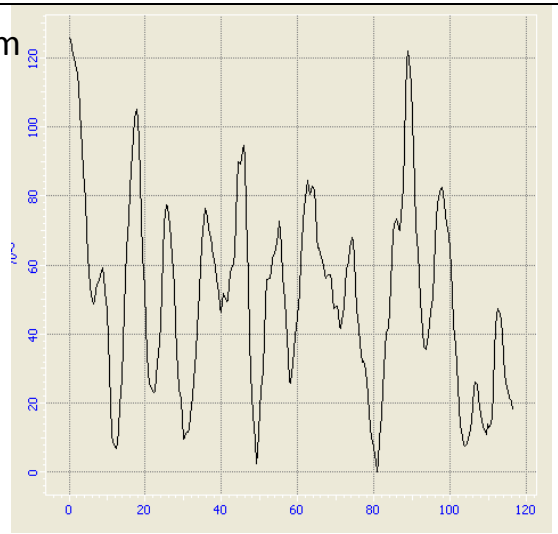	0.026
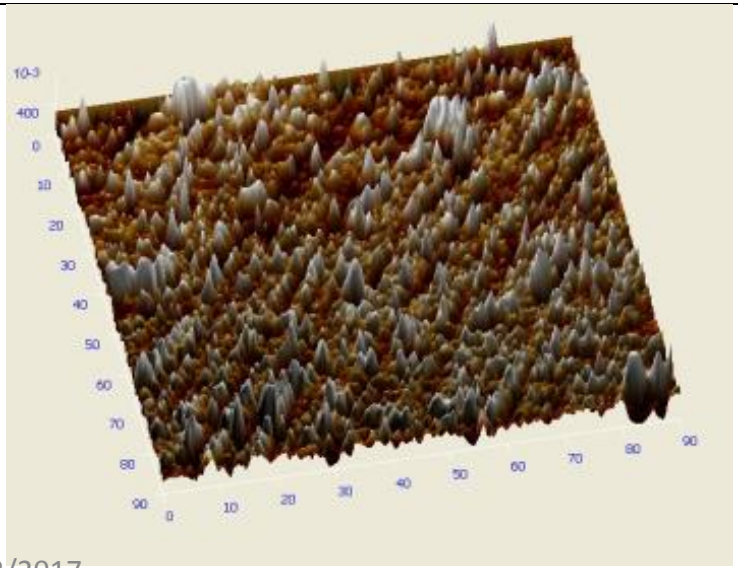	1.0 μm 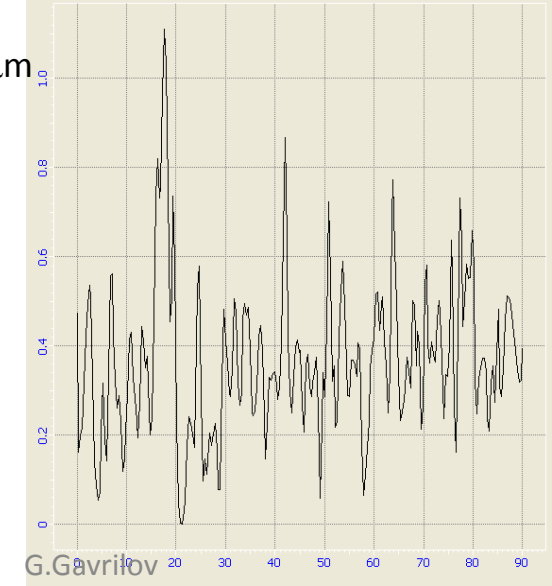	0.123

Sample E-H

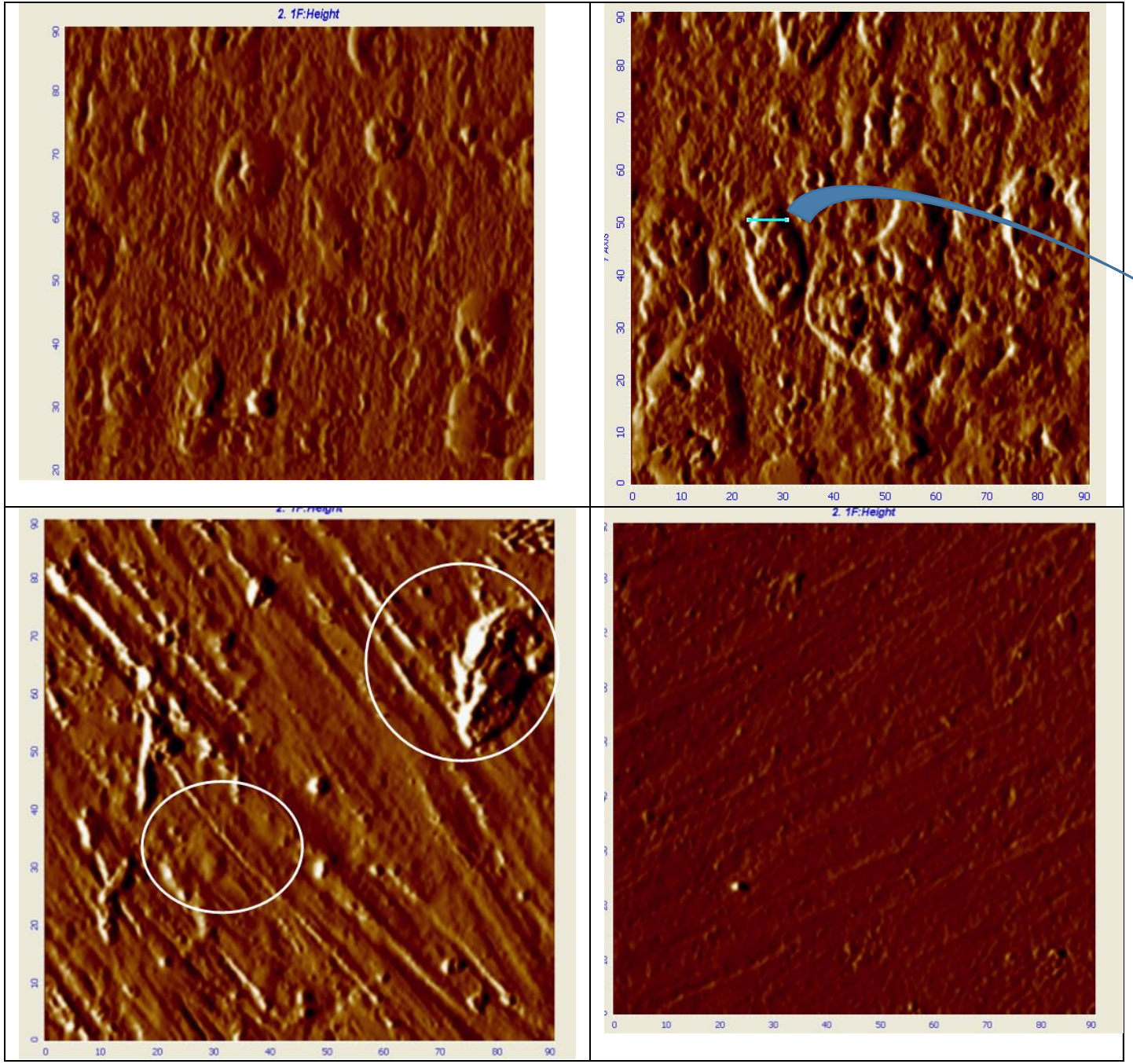

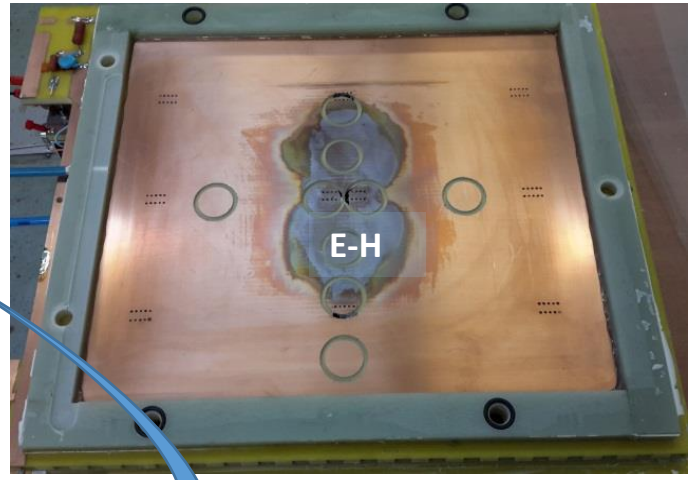

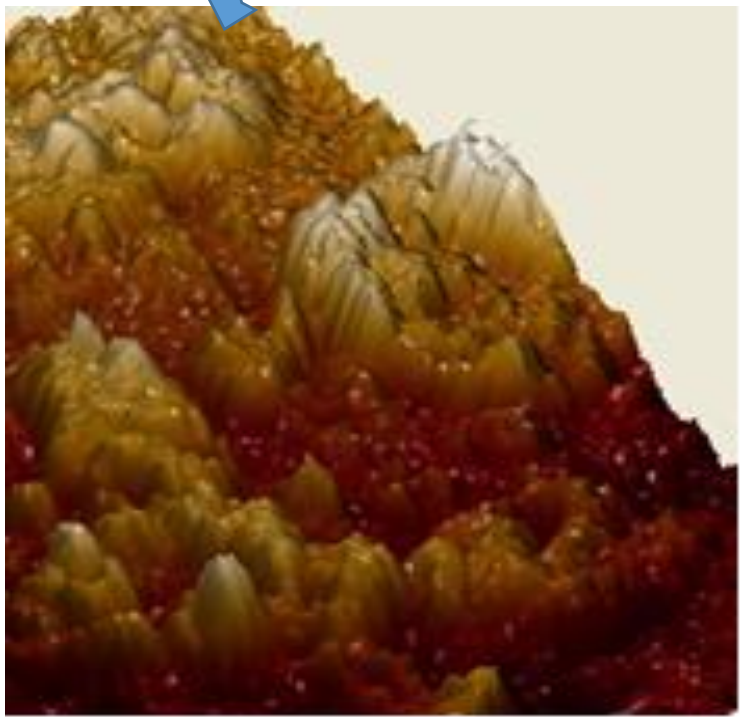

3 × 3 μm

A crater after blister explosion

Sample E^f

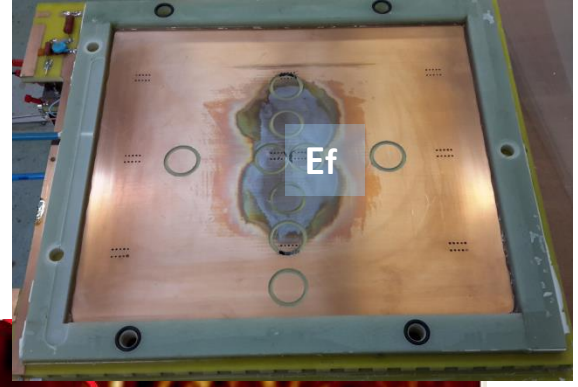

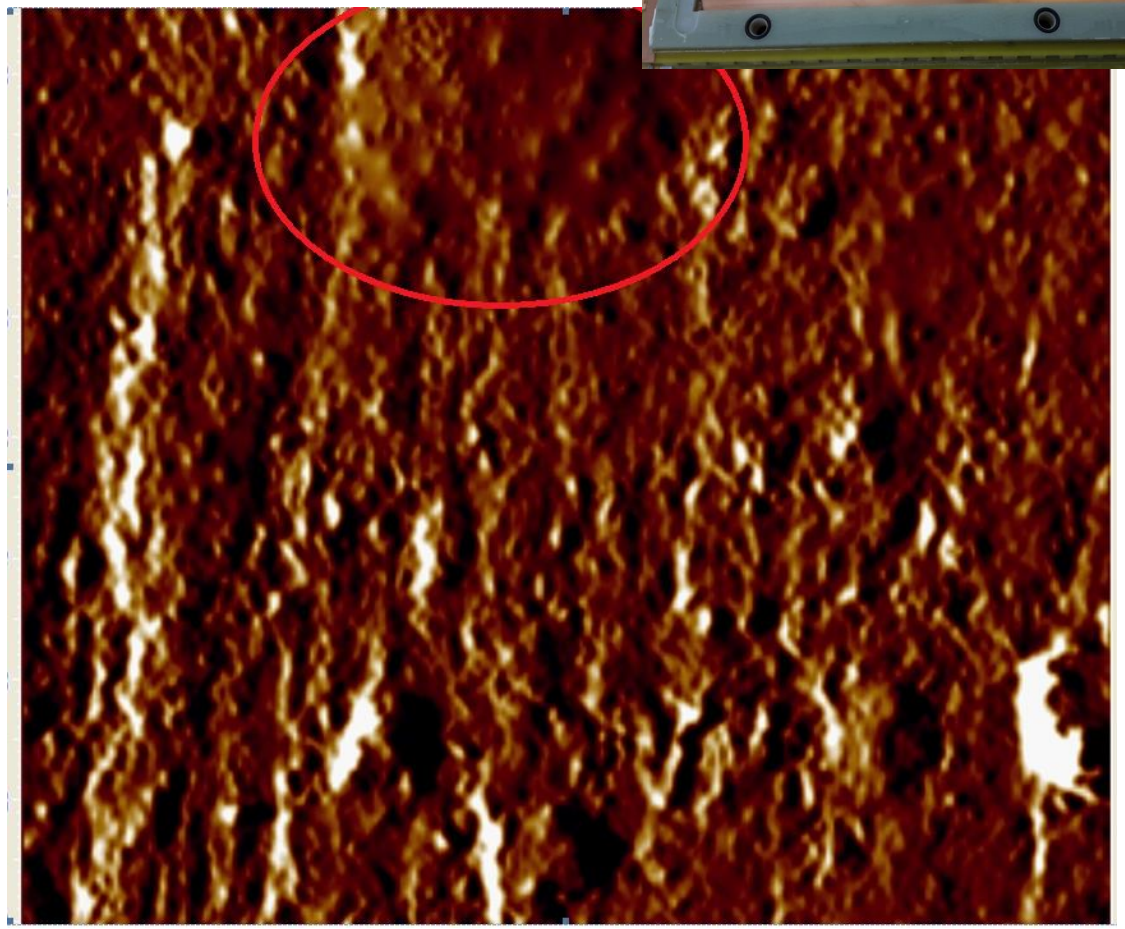

Sample H

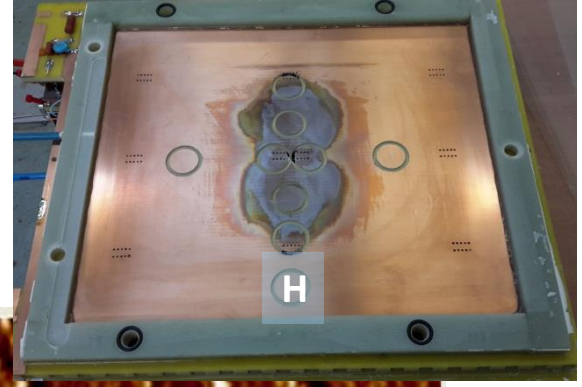

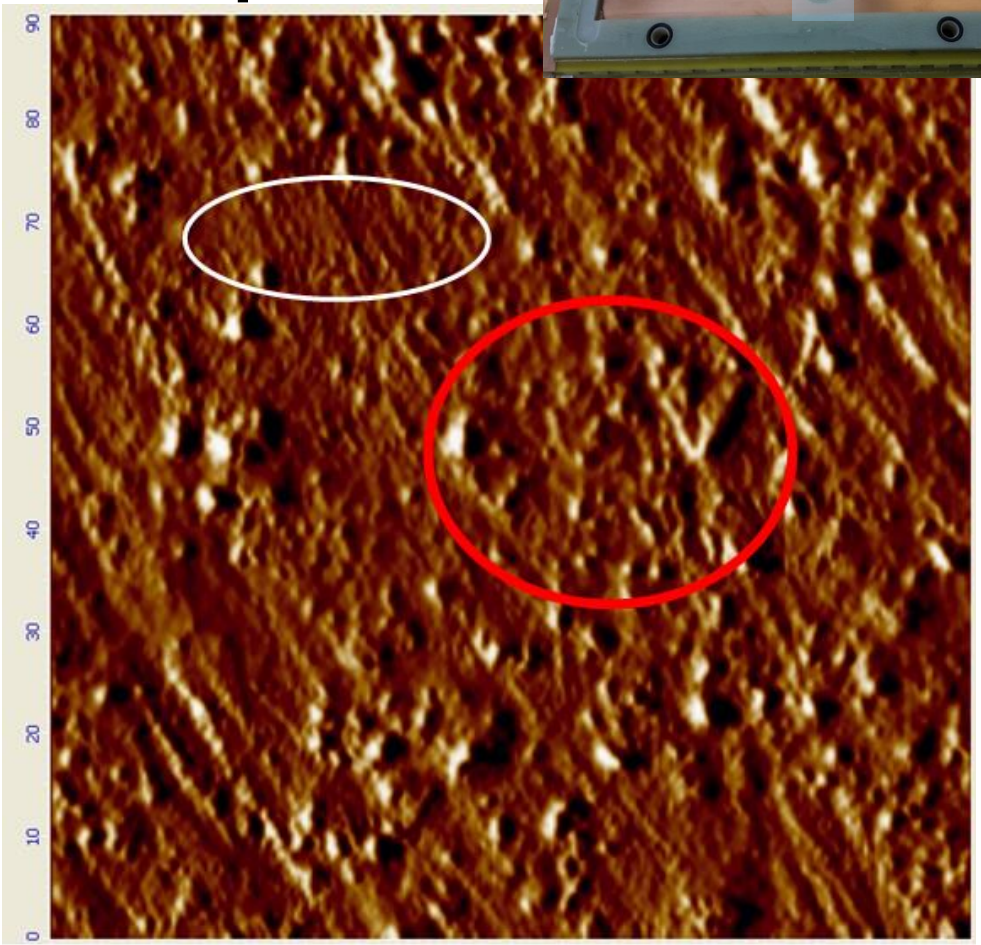

Sample C - porosity evaluation procedure

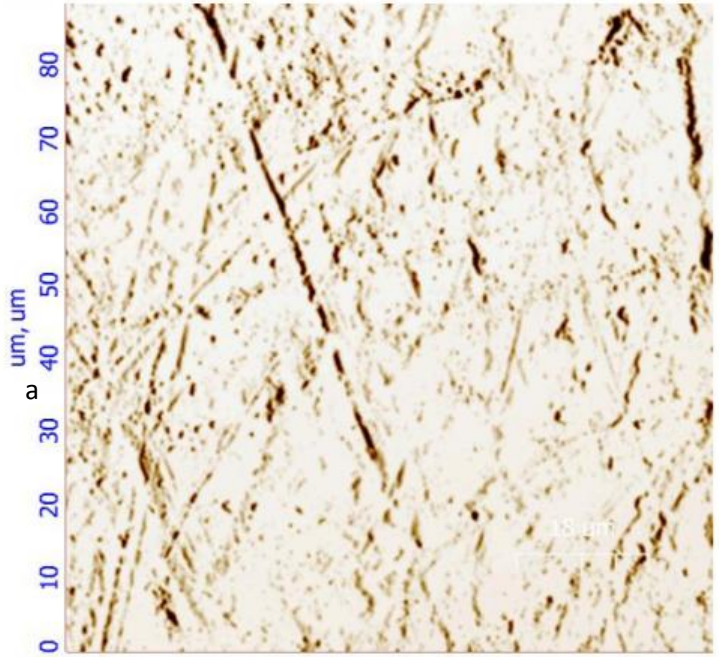

a

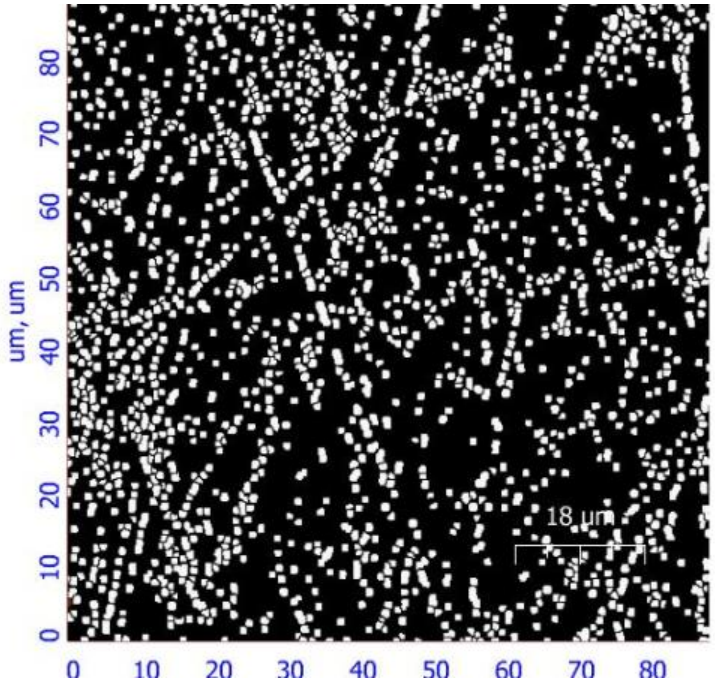

b

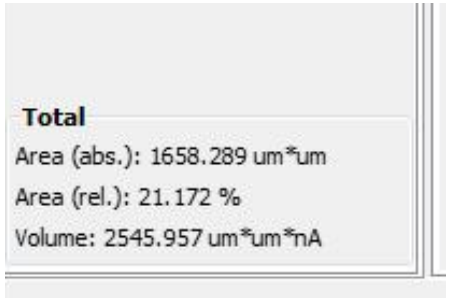

c

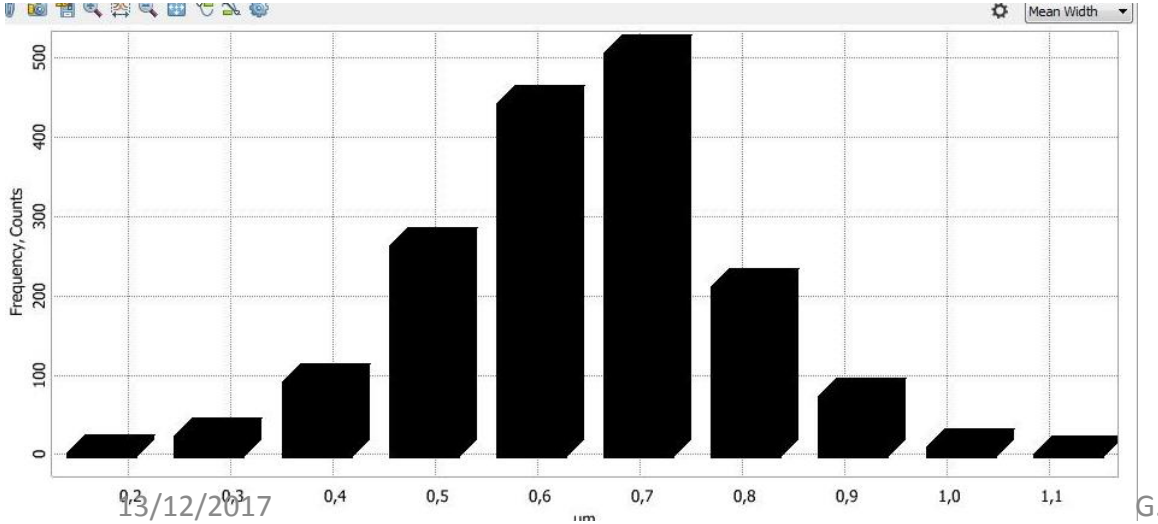

d

«Grain analysis» program

a. image preparation for processing;
b. pore release;
c. result;
d. resulting histogram.

Porosity distribution in the samples

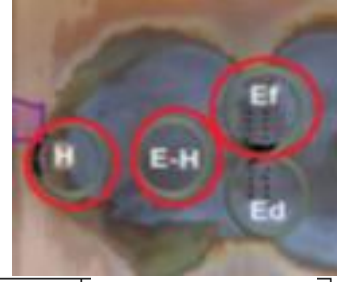

Sample	Histogram	Area of porous space, %
C	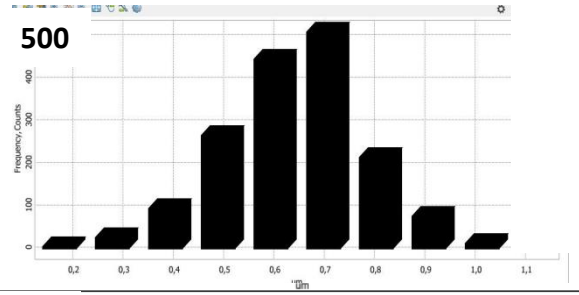	17
E-D	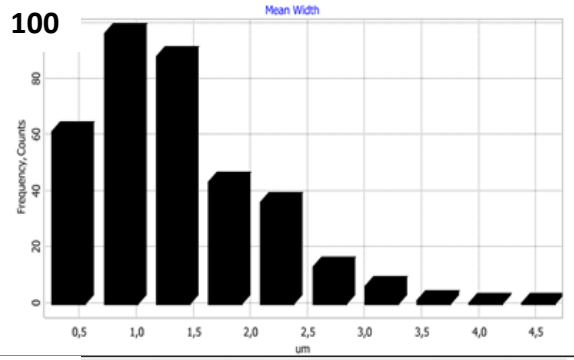	30,9
H	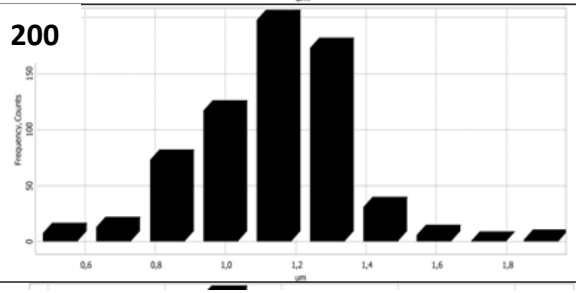	22

Sample	Histogram	Area of porous space, %
E-H	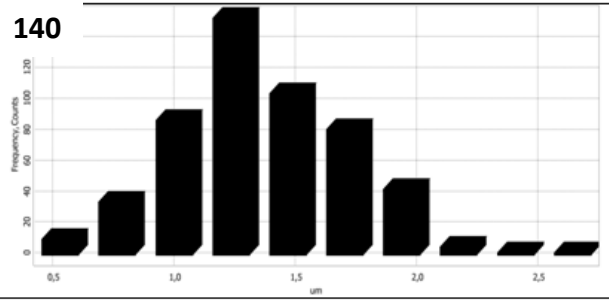	31,7
E^f	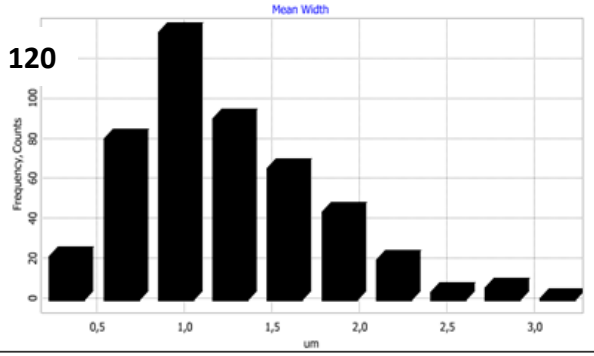	30.8

- Most of porous has diameter 1.0-1.5 μm
- In the “reference” point C the porous size is smaller then in the rest samples - 0.7 μm

Nuclear scanning microprobe analysis of the samples

Vary of concentration of the **Oxygen** *in the* **Cooper** *foil with a depth of the analysed layer for different samples*

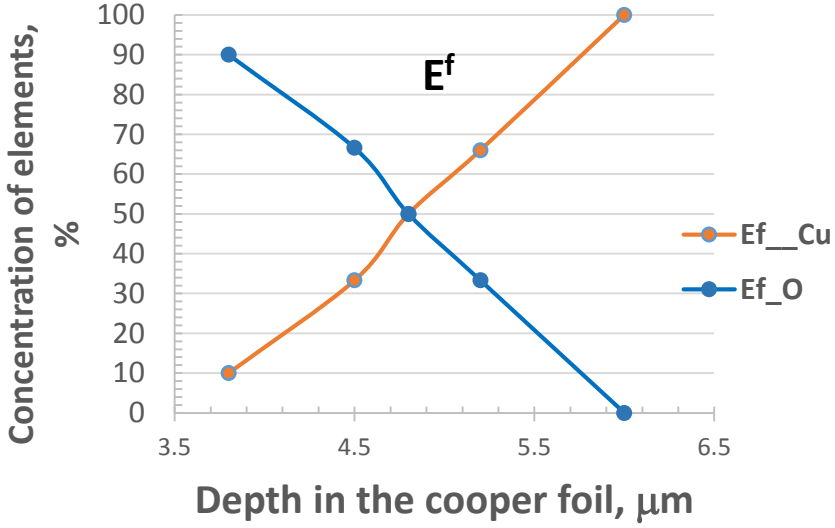

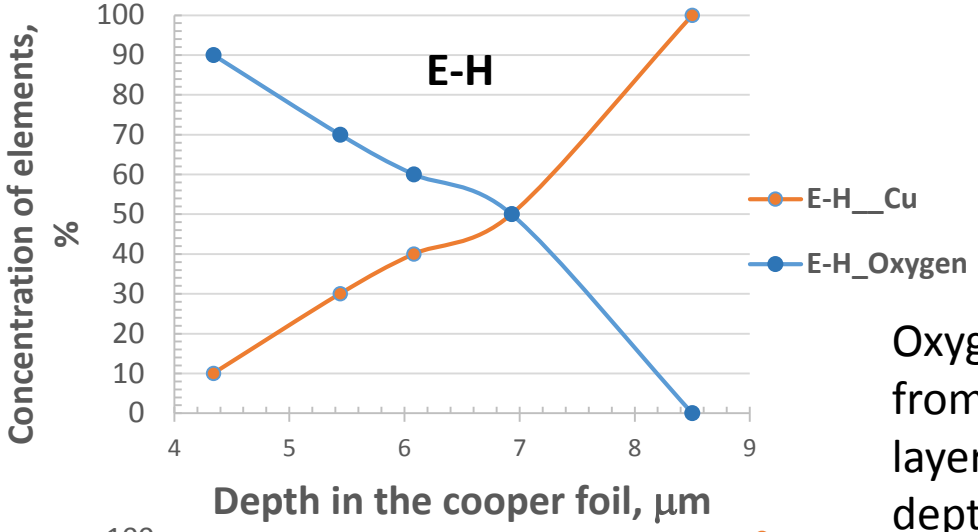

Oxygen concentration changes from 90% at the 3 µm surface layer up to 0% on the 6-10 µm depth in the cooper foil

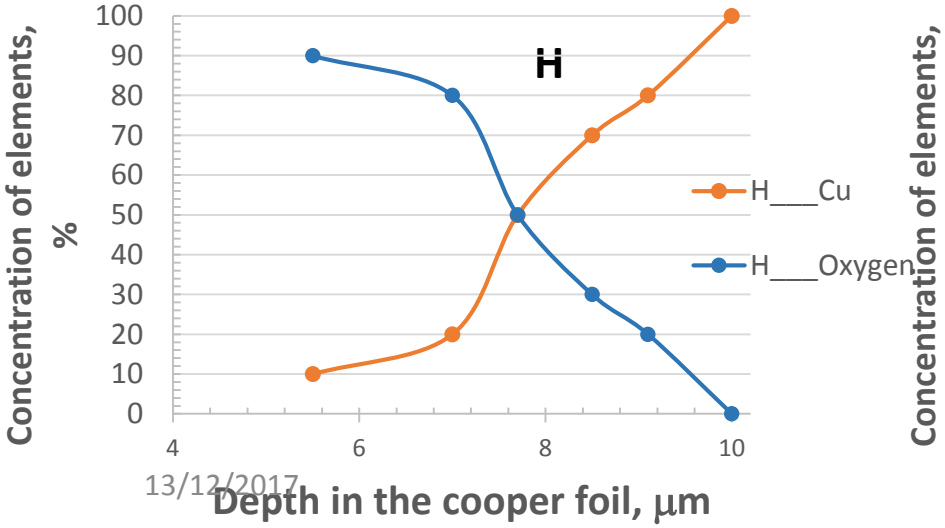

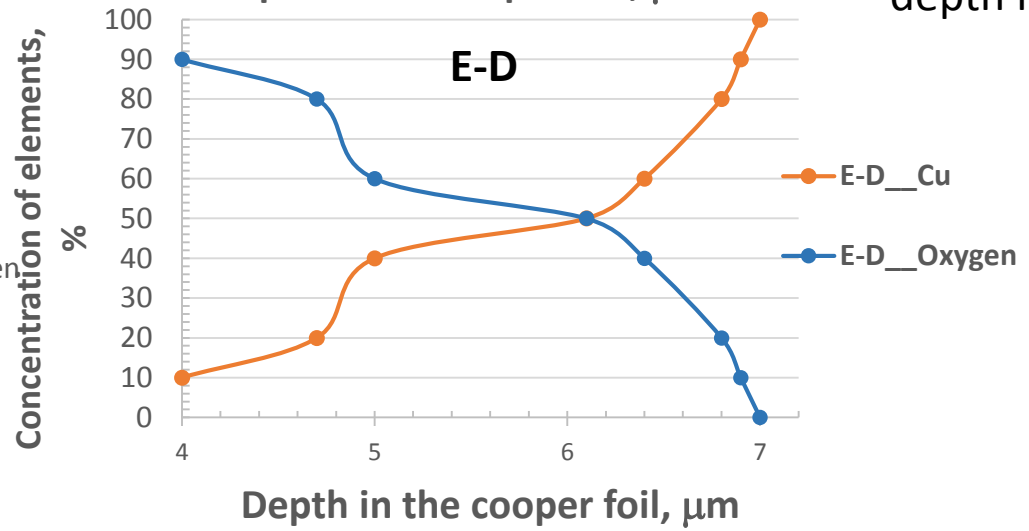

Summary & Outlook

- Oxygen radicals and molecules play a key role in the damage of the cathode copper causing the blisters grow and roughness increase
- At early stage of Cu oxidation (Cu_2O - cuprous oxide) when surface resistance is high an appearance of Malter current is very probable
- While the cooper oxidation continues up to the conductive CuO - cupric oxide - the probability of Malter effect decreases
- An accurate surface resistance measurement is needed for the samples of aged CSC prototypes
- More systematic study of the damaged cooper foil with an atomic force microscopy and microzond is planned

Backups

Backups

Sample E-H

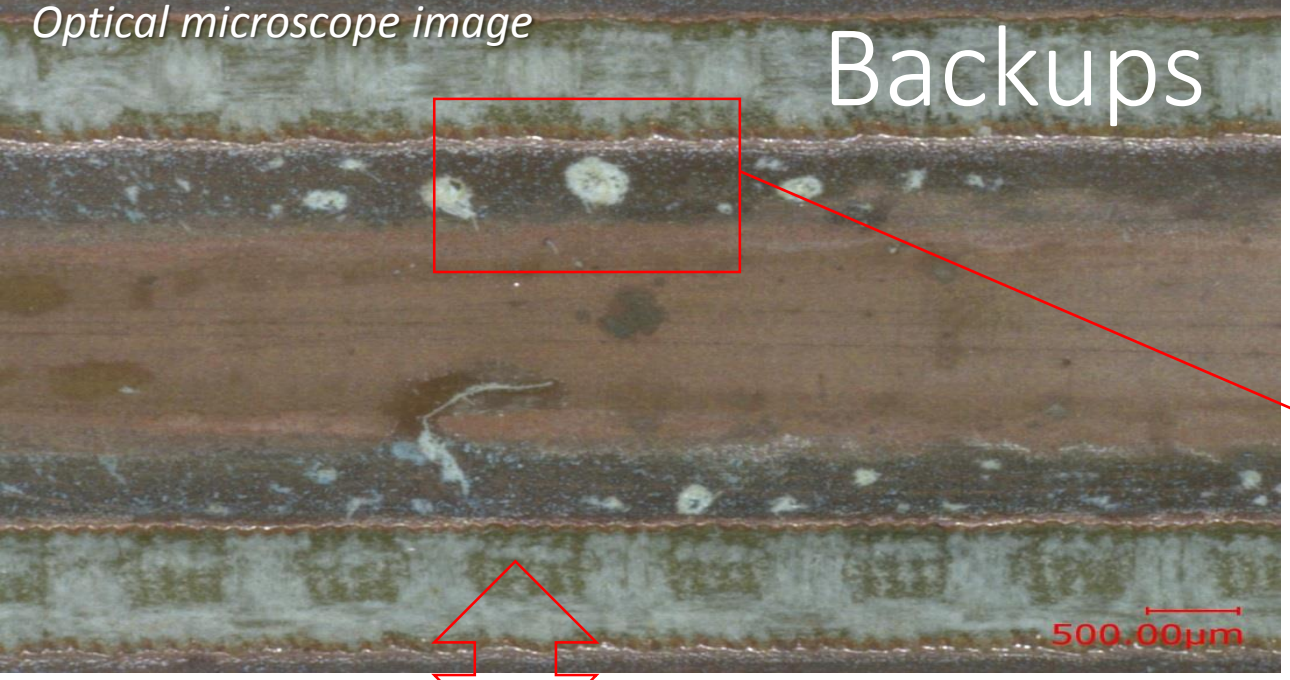

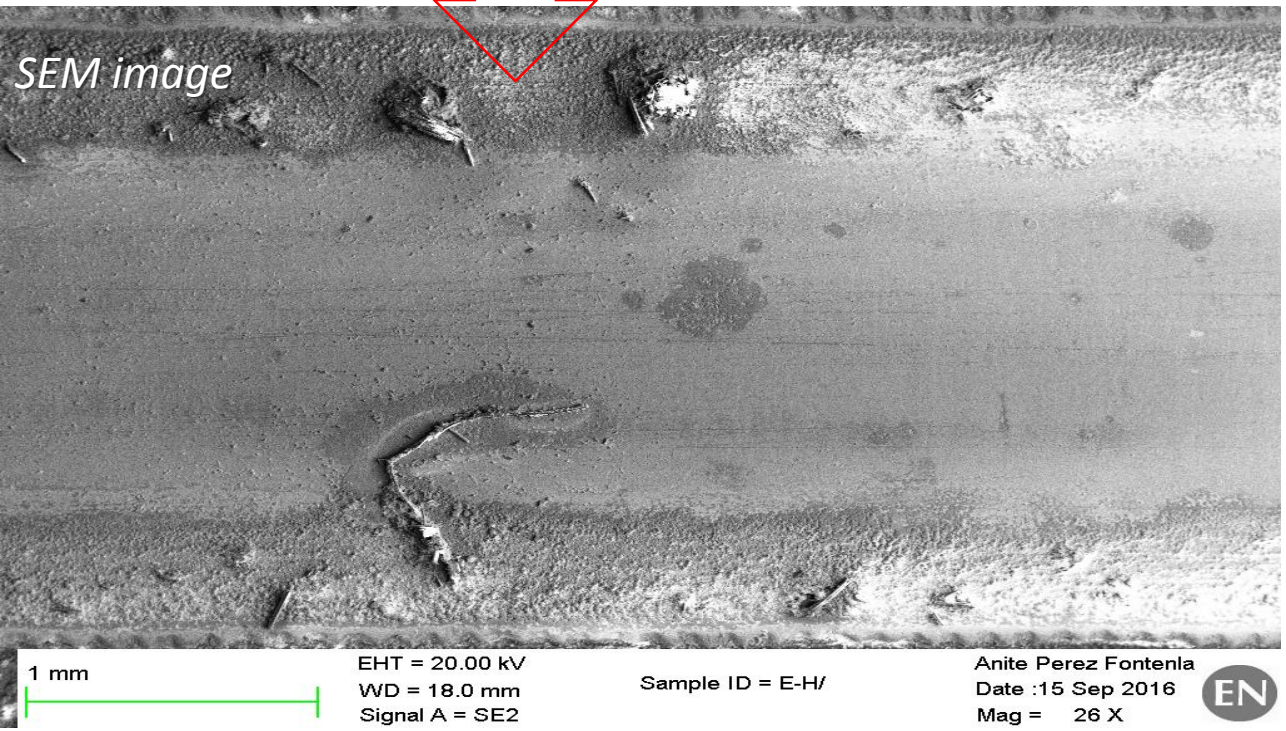

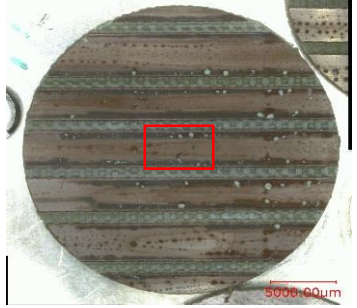

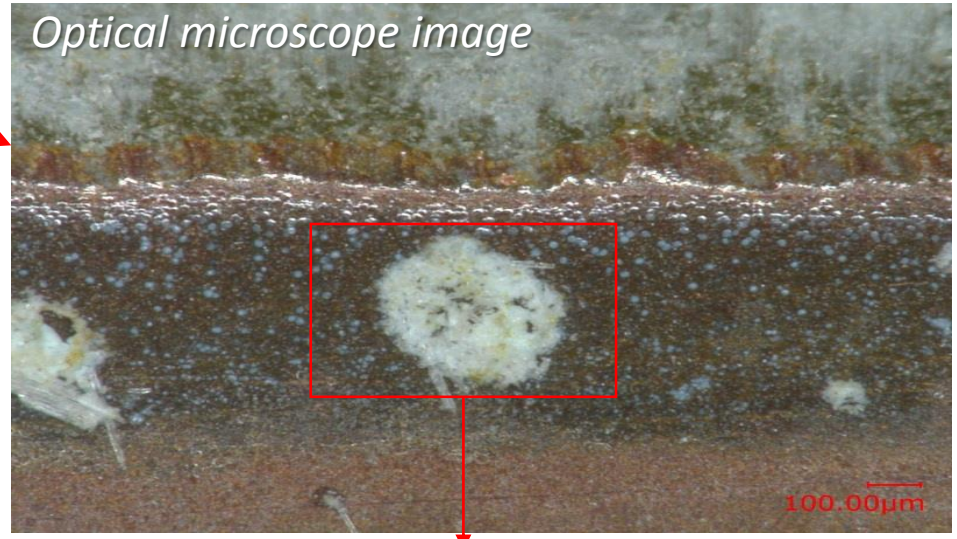

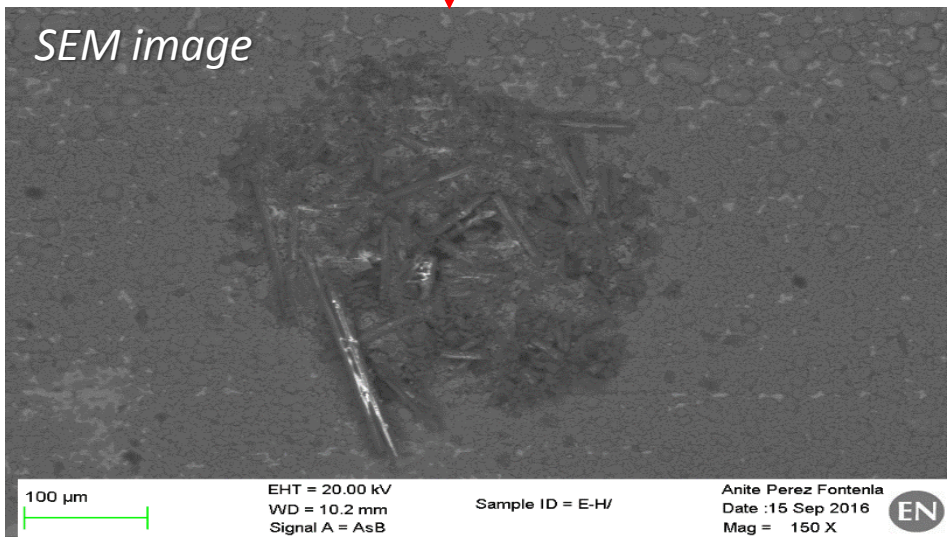

Nuclear scanning microprobe analysis with EGP-10

Considering the kinematics of the collision (that is, the conservation of momentum and kinetic energy), the energy E_1 of the scattered projectile is reduced from the initial energy E_0: $E_1 = K(\theta) \times E_0$, where $K(\theta)$ is known as the *kinematical factor*,

To measure backscattered energy the Si surface barrier detector is used.
Ions which reach the detector lose some of their energy to inelastic scattering from the electrons.
Number of electron-hole pairs produced in the detector is dependent on the energy of the ion.

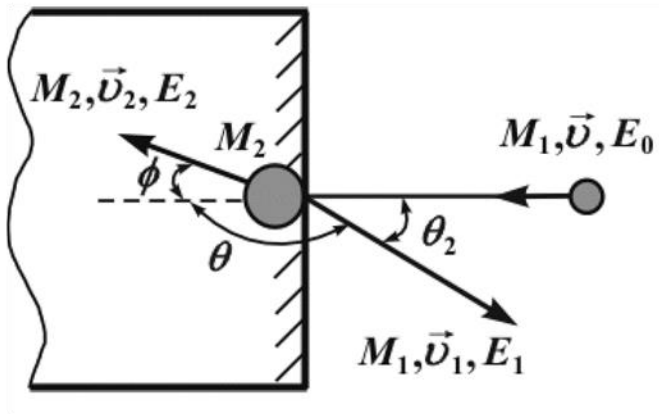

$$\theta = 180 - \theta_2;$$

$$K(\theta) = \left[\frac{\sqrt{\frac{M_2^2}{M_1^2} - 1 + \cos^2\theta} + \cos\theta}{\frac{M_2}{M_1} + 1} \right]^2$$

L. De Los Santos Valladares et al., Crystallization and electrical resistivity of Cu2O and CuO obtained by thermal oxidation of Cu thin films on SiO2/Si substrates, Thin Solid Films 520 (2012) 6368–6374

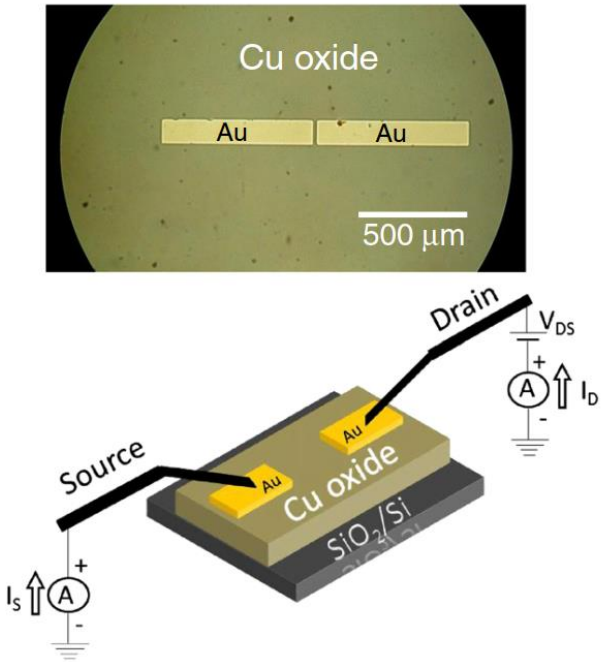

Fig. 1. Optical microscope image of two gold strips evaporated on a Cu oxide film (top), and schematic representation of the configuration for the electrical measurements (bottom).

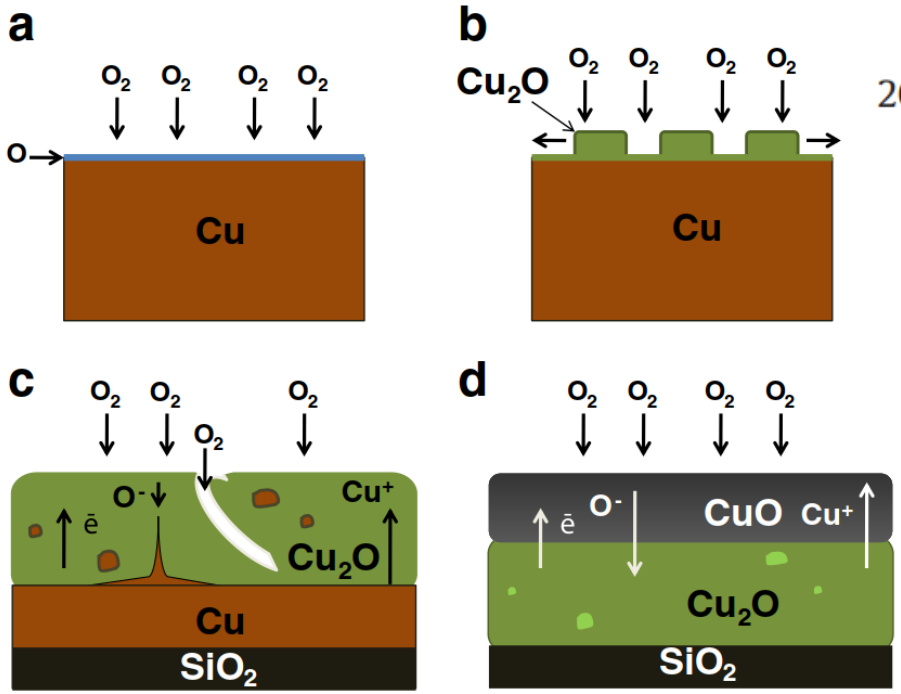

$$2Cu + 1/2O_2 \rightarrow Cu_2O.$$

$$Cu_2O + 1/2O_2 \rightarrow 2CuO.$$

Fig. 3. Representation of the oxidation mechanism of the surface on a copper film.

Summary for XRD data of copper oxide films obtained by thermal oxidation.

Annealing temperature (°C)	Phase	(hkl)	2θ (°)	Crystallite size (nm)
RT	Cu	(111)	43.43	19
	Cu	(200)	50.60	–
150	Cu	(111)	43.43	21
	Cu	(200)	50.60	–
	Cu_2O	(111)	36.35	6
	Cu_2O	(200)	42.70	–
200	Cu_2O	(111)	36.35	13
	Cu_2O	(200)	42.70	–
250	Cu_2O	(111)	36.74	14
	CuO	(111)	38.63	9
	CuO	$(\bar{1}11)$	35.50	–
275	Cu_2O	(111)	36.63	15
	CuO	(111)	38.74	17
	CuO	$(\bar{1}11)$	35.50	–
300	CuO	(111)	38.86	21
	CuO	$(\bar{1}11)$	35.70	–
900	CuO	(111)	38.95	35
	CuO	$(\bar{1}11)$	35.70	–
1000	CuO	(111)	39.05	40
	CuO	$(\bar{1}11)$	35.56	–

Flora M. Li et al., Low temperature (<100 °C) deposited P-type cuprous oxide thin films: Importance of controlled oxygen and deposition energy, Thin Solid Films 520 (2011) 1278–1284

Copper forms two types of oxides: cuprous oxide (Cu_2O) and cupric oxide (CuO), each with unique material properties as highlighted in Table 1. Cu_2O is a highly transparent, yellow, p-type semiconductor, while CuO is typically an opaque, more conductive material. Although Cu_2O is the native oxide of copper, it is often difficult to form pure Cu_2O films and requires precise control of the stoichiometry. Even moderate excess of oxygen and/or reaction energy tends to favour the formation of CuO instead of Cu_2O. Fig. 1 provides a simplified illustration of the oxidation pathway to form Cu_2O and CuO from copper.

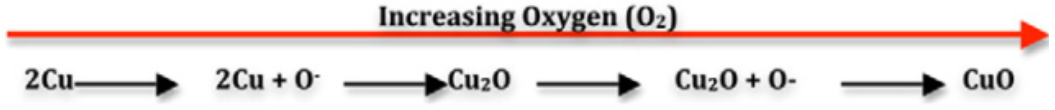

Fig. 1. Simplified illustration of the oxidation reaction of copper for the formation o Cu_2O and CuO.

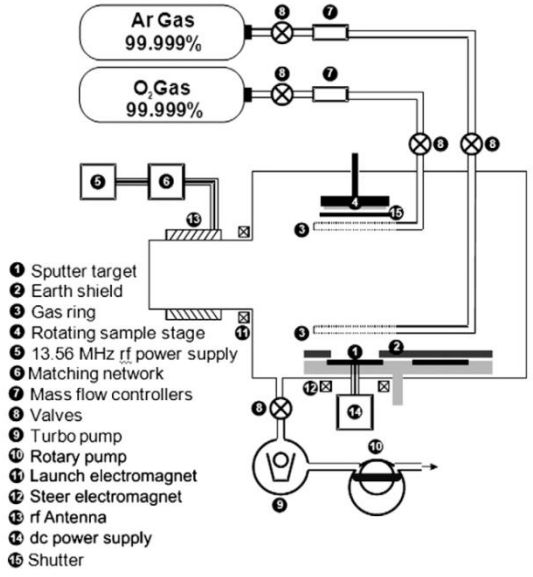

Fig. 2. Schematic illustration of a HiTUS sputtering system, with a remote plasma chamber where the substrate/sample is removed from the sputtering plasma. Illustration adapted from Ref. [13].

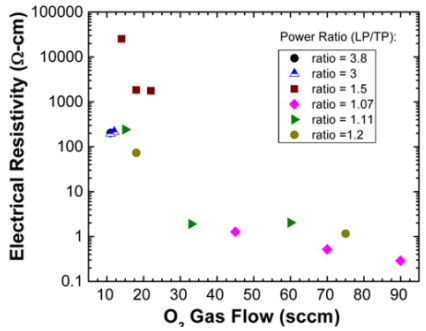

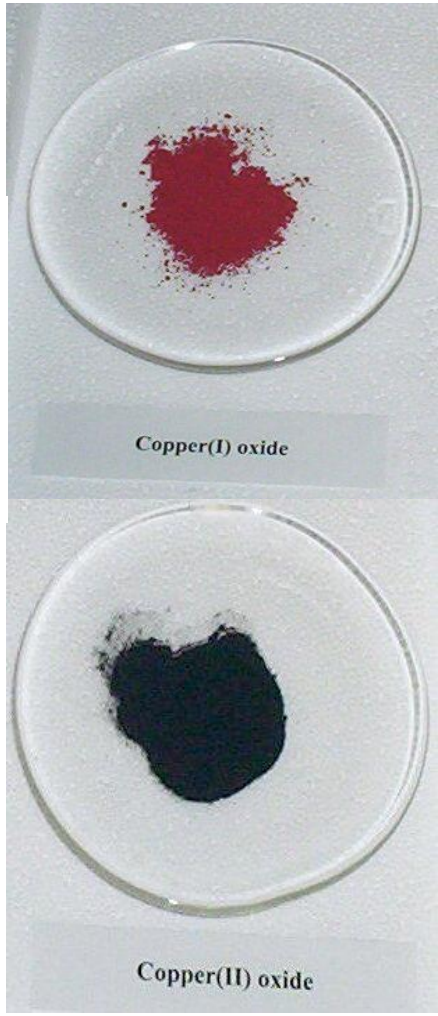

Table 1
Comparison of the different oxides of copper [3,6].

Name	Molecular formula	IUPAC name	E_g (eV)	Resistivity (Ω-cm)	Type	Crystal structure	Appearance
Cuprous oxide	Cu_2O	Copper (I) oxide	2.0–2.6	10^3–10^8	P	Cubic	Yellow/Red, semi-transparent
Cupric oxide	CuO	Copper (II) oxide	1.2–1.6	0.01–1	N/P	Monoclinic	Darker colour